

5-2024

EVALUATION OF AN END-TO-END RADIOTHERAPY TREATMENT PLANNING PIPELINE FOR PROSTATE CANCER

Mohammad Daniel El Basha

The University of Texas MD Anderson Cancer Center UTHealth Graduate School of Biomedical Sciences,
mdelbasha@gmail.com

Court Laurence

The University of Texas Graduate School of Biomedical Sciences at Houston

Carlos Eduardo Cardenas

The University of Texas M D Anderson Cancer Center UTHealth Graduate School of Biomedical Sciences


Julianne Pollard-Larkin

The University of Texas MD Anderson Cancer Center UTHealth Graduate School of Biomedical Sciences

Steven Frank

Follow this and additional works at: https://digitalcommons.library.tmc.edu/utgsbs_dissertations

The University of Texas MD Anderson Cancer Center

 Part of the [Artificial Intelligence and Robotics Commons](#), [Data Science Commons](#), [Medical Biophysics Commons](#), [Oncology Commons](#), [Other Physics Commons](#), and the [Radiation Medicine Commons](#)
See next page for additional authors

Recommended Citation

El Basha, Mohammad Daniel; Laurence, Court; Cardenas, Carlos Eduardo; Pollard-Larkin, Julianne; Frank, Steven; Fuentes, David T.; Poenisch, Falk; and Yu, Zhiqian H., "EVALUATION OF AN END-TO-END RADIOTHERAPY TREATMENT PLANNING PIPELINE FOR PROSTATE CANCER" (2024). *Dissertations & Theses (Open Access)*. 1347.

https://digitalcommons.library.tmc.edu/utgsbs_dissertations/1347

This Thesis (MS) is brought to you for free and open access by the MD Anderson UTHealth Houston Graduate School at DigitalCommons@TMC. It has been accepted for inclusion in Dissertations & Theses (Open Access) by an authorized administrator of DigitalCommons@TMC. For more information, please contact digcommons@library.tmc.edu.

Author

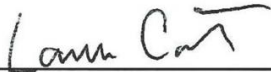
Mohammad Daniel El Basha, Court Laurence, Carlos Eduardo Cardenas, Julianne Pollard-Larkin, Steven Frank, David T. Fuentes, Falk Poenisch, and Zhiqian H. Yu

EVALUATION OF AN END-TO-END RADIOTHERAPY TREATMENT PLANNING
PIPELINE FOR PROSTATE CANCER

By

Mohammad Daniel El Basha, B.S.

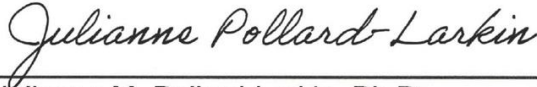
APPROVED:



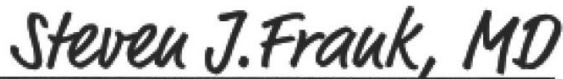
Laurence E. Court, Ph.D.
Supervisory Professor



Carlos E. Cardenas, Ph.D.



Julianne M. Pollard-Larkin, Ph.D.



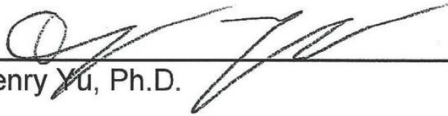
Steven J. Frank, M.D.



David T. Fuentes, Ph.D.

Falk Poenisch

Falk Poenisch, Ph.D.



Henry Yu, Ph.D.

APPROVED:

Dean, The University of Texas
MD Anderson Cancer Center UTHealth Houston Graduate School of Biomedical Sciences

EVALUATION OF AN END-TO-END RADIOTHERAPY TREATMENT PLANNING
PIPELINE FOR PROSTATE CANCER

A
THESIS

Presented to the Faculty of
The University of Texas
M.D. Anderson Cancer Center UTHealth Houston
Graduate School of Biomedical Sciences
in Partial Fulfillment
of the Requirements
for the Degree of

MASTER OF SCIENCE

By
Mohammad Daniel El Basha, B.S.
Houston, Texas

May 2024
Copyright (c) 2024 Mohammad Daniel El Basha. All rights reserved.

ACKNOWLEDGMENTS

I want to thank my advisor, Dr. Laurence Court, for his immense support and encouragement throughout my master's journey. Thank you for your patience, care, and commitment to seeing me through this project.

I want to thank my committee, Drs. Carlos Cardenas, David Fuentes, Julianne Pollard-Larkin, Henry Yu, Steven Frank, and Falk Poenisch, thank you for your wisdom and invaluable input during every individual meeting, committee meeting, and beyond. Your time, energy, and advice invested into this project have shaped me as a researcher and directed me on my journey.

Thank you to all the present members and alums of the Courtlab for fostering a creative, loving, and supportive research environment. You are all exceptional individuals, which makes this lab a wonderful place to impact not only patients' lives but peoples' lives, too. Your critical feedback during abstract and presentation review sessions, encouragement, and guidance on navigating graduate school life have contributed immensely to my development and success.

With the deepest of love and appreciation, I thank all my friends here in Houston, Florida, and wherever they find themselves. Their supportive messages, care packages, long-distance and late-night calls, impromptu walk-ins, and tender hugs gave me the strength and support necessary to persist through the ups and downs I encountered throughout graduate school.

Finally, I want to thank my parents and family for always caring about every aspect of my life. From decisions in graduate school to how I went about my day, they were always there and reminded me that God would be with me every step of the way, and he has. Your love and sacrifice have been my anchor and shelter, providing me with inspiration and energy to grow. I am grateful for your love and support, which have with God led me all this way.

EVALUATION OF AN END-TO-END RADIOTHERAPY TREATMENT PLANNING PIPELINE FOR PROSTATE CANCER

Mohammad Daniel El Basha, B.S.

Advisory Professor: Laurence E. Court, Ph.D.

Radiation treatment planning is a crucial and time-intensive process in radiation therapy. This planning involves carefully designing a treatment regimen tailored to a patient's specific condition, including the type, location, and size of the tumor with reference to surrounding healthy tissues. For prostate cancer, this tumor may be either local, locally advanced with extracapsular involvement, or extend into the pelvic lymph node chain. Automating essential parts of this process would allow for the rapid development of effective treatment plans and better plan optimization to enhance tumor control for better outcomes.

The first objective of this work, to automate the treatment planning process, was the automatic segmentation of critical structures. Delineation of both target and normal tissue structures was necessary to establish the foundation for identifying where radiation must be delivered and what should be spared from excess radiation.

Deep learning segmentation models were developed from retrospective CT simulation imaging data and clinical contours to delineate intact, postoperative, and nodal treatment structures for prostate cancer to accomplish this objective. Quality contours were extracted per established contouring guidelines in the literature. Model refinement on a holdout fine-tune dataset was used to verify model contours before quantitative and qualitative evaluation on the holdout test set. Predicted contours resulted in contours comparable in quantitative Dice-Similarity-Coefficient (DSC) and 95% Hausdorff Distance (HD95) to proposed models in literature and clinically usable contours with no more than minor edits upon physician review.

The second objective was the automation of Volumetric Modulated Arc Therapy (VMAT) planning for a breadth of prostate treatment scenarios. Development of VMAT plans for intact, postoperative, and nodal involvement treatment cases was necessary for the sequence in daily

treatment delivery and the prospective distribution of radiation dose to target and normal tissues.

To accomplish this objective, knowledge-based planning models were separately developed to estimate patient-specific DVHs to guide plan optimization for radiation delivery. These two models were then used in this work for end-to-end testing of cases with and without lymph node involvement, including determining if the prostate target is intact or postoperative with or without treatment devices such as hydrogel spacers and rectal balloons. A sequence of iterative optimization runs was created to ensure hotspot reduction and target conformality.

The findings demonstrated that plans developed from automatically generated contours were clinically usable with minor edits for intact and postoperative treatments without lymph node involvement. For treatments with lymph node involvement, dose constraints were met for a select set of cases without excessive rectum curvature or excessive bladder descension into the postoperative treatment bed. When comparing auto-segmented to clinical contours, clinical contours experienced similar pass rates as those achieved by auto-segmented contours.

TABLE OF CONTENTS

Approval Page	i
Title Page	ii
Acknowledgments.....	iii
Abstract	iv
Table of Contents	vi
List of Figures	viii
List of Tables	x
Chapter 1: Introduction	1
Chapter 2: Central Hypothesis and Specific Aims	5
Chapter 3: Automated contouring system for prostate cancer using deep learning frameworks	6
Introduction	6
Methods	8
Patient Dataset	8
Contour Model Development	11
Preparation of data for contour model training.....	11
Model Training	12
Post Processing	14
Contour Evaluation.....	16
Results	16
Discussion.....	24

Conclusion	27
Chapter 4: Automated knowledge-based planning for prostate cancer	29
Introduction	29
Methods	31
VMAT plan data	31
Automated Planning Strategy	32
Auto-Plan Evaluation	33
End-to-End Evaluation	34
Results	35
Model Evaluation	35
End-to-End Evaluation	38
Discussion	42
Conclusion	43
Chapter 5: Discussion and Conclusion	45
Project Summary	45
Study Limitations and Future Directions	47
Conclusion	49
Bibliography	50
Vita	62

LIST OF FIGURES

Figure 1 Illustration of contouring the aortic bifurcation as the support structure for lymph node CTV contouring according to NRG guidelines.	10
Figure 2 U-Net architecture was customized for the segmentation of structures by the nnU-Net Framework based on available training data.	12
Figure 3 Workflow of combining model predictions from clinical data to create a complete training contour set of deep learning predictions. From the targets and OARs deep learning prediction dataset, the final two targets and OAR nnU-Net models are trained to contour respective structures. The numbering on the left-hand side corresponds to the Model ID in Table 3.....	14
Figure 4 Boundary correction was performed on generated segmentations of model predictions. An example of an auto-contoured rectum and sigmoid prediction being reset to the median overlapping slice from the contour boundaries' most inferior and superior borders.	15
Figure 5 Boxplot of the distribution in DSC scores between predicted structures from individual, ensemble, and the proposed multi-class segmentation models	17
Figure 6 Box and whisker plots of Dice similarity coefficient (DSC) between ground-truth and automatically generated contours.....	18
Figure 7 Qualitative review of 45 sets of patient contours on CT by three radiation oncologists for planning structures of intact and postop treatment cases. Each physician reviewed 15 intact and postop cases in total.	20
Figure 8 Qualitative review of 20 sets of patient contours on CT by two radiation oncologists for planning structures of intact and postop treatment cases. Each physician reviewed ten intact and postop cases in total.	20
Figure 9 Visual comparison of qualitative physician scoring for predicted contours (cyan) to clinical ground truth contours (magenta) for organs at risk: rectum, sigmoid, and bladder.....	21

Figure 10 Visual comparison of qualitative physician scoring for predicted contours (cyan) to clinical ground truth contours (magenta) for target structures: prostate, seminal vesicles, prostate bed, SV-fossa, and lymph node CTV. 22

Figure 11 Visualization of automated treatment plans from Prostate only RadidPlan... 39

LIST OF TABLES

Table 1 Summary of contouring guidelines observed to curate ground truth data for deep learning model development.....	9
Table 2 Target, organs-at-risk (OARs), and other structures automatically contoured within our treatment pipeline, separated by structures from newly developed models and structures adopted from established models.	11
Table 3 Summary of contouring models developed on a treatment-case basis.....	14
Table 4 The table details the 5-point scale for evaluating the quality of generated auto-contours and auto-plans.....	16
Table 5 Mean Dice similarity coefficient (DSC), surface DSC, 95% Hausdorff Distance (HD95), and mean surface distance (MSD) between ground truth and prediction results for our auto-contouring models.....	19
Table 6 Comparison of deep learning model segmentation performance to other CT-based contour prediction models in the literature. * Reference reported Hausdorff Distance rather than HD95; ** Structure is not explicitly segmented or is considered part of a larger structure.....	26
Table 7 Prostate and Pelvic Lymph node target and normal tissue clinical treatment planning goals.....	33
Table 8 Qualitative scoring of physician review prostate only and prostate & nodes RapidPlan VMAT treatment plans.	36
Table 9 Summary for auto-plans meeting, within 5% of or greater than 5% of dosimetric recommendations on manually drawn contour set for four radiation treatment prescriptions: three on prostate and seminal vesicle targets for 78, 72, and 60 Gy and one on the prostate bed and SV-fossa targets for 70 Gy.	37
Table 10 Summary for auto-plans meeting, within 5% of or greater than 5% of dosimetric recommendations on manually drawn contour set for two radiation treatment	

prescriptions on prostate and lymph node targets: 70 & 50.4Gy in 35 fractions and 59.8 & 46Gy in 35 fractions..... 38

Table 11 Summary for auto-plans meeting, within 5% of or greater than 5% of dosimetric recommendations on auto-contours and clinical contours with radiation treatment prescription on Prostate and seminal vesicle targets of 78Gy in end-to-end testing of treatment pipeline..... 40

Table 12 Summary for auto-plans meeting, within 5% of or greater than 5% of dosimetric recommendations on auto-contours and clinical contours with radiation treatment prescription on Prostate Bed and SV-Fossa targets of 70Gy in end-to-end testing of treatment pipeline..... 41

Table 13 Summary for auto-plans meeting, within 5% of or greater than 5% of dosimetric recommendations on auto-contours and clinical contours with radiation treatment prescription on prostate and lymph node targets of 70 & 50.4Gy in end-to-end testing of treatment pipeline..... 42

CHAPTER 1: INTRODUCTION

Prostate cancer remains a significant health concern in men worldwide, representing the second most diagnosed cancer among men in the US and the fifth leading cause of cancer-related deaths globally (Sung et al., 2021). For disease incidence, prostate cancer ranks second in higher human development index countries (a composite measure of life expectancy, education, and per capita income) with 37.5 new cases per 100,000 men. It is estimated that 1 in 8 men will be diagnosed with prostate cancer in their lifetime. This is in tandem with increases in prostate cancer by 3% annually from 2014 to 2019. In 2023, it is estimated that there will be over 288,000 new cases in the US alone (Siegel et al., 2023). Despite advancements in diagnosis and treatment, the management of prostate cancer poses numerous challenges due to its heterogeneity in presentation, varying clinical courses, potential for recurrence, and socioeconomic factors of treatment access (Gray et al., 2017). Among the multitude of treatment options available, radiation therapy serves as a key treatment paradigm for prostate cancer, offering curative potential while preserving functional outcomes and quality of life for men.

In recent years, integrating deep learning techniques, particularly image segmentation algorithms, has emerged as a promising technology to further the advancement of treatment planning and delivery in prostate cancer. Deep learning-based image segmentation can revolutionize the delineation of target volumes and organs at risk, thereby improving the precision and accuracy of radiation therapy delivery while minimizing unnecessary radiation exposure to surrounding healthy tissues. Automation of segmentation also increases consistency in tissue boundary definitions, thereby reducing contour variability and the time necessary to outline boundaries, resulting in increased efficiency across clinical workloads (Baroudi et al., 2023). Deep learning algorithms can discern intricate patterns and features within medical images by learning from vast amounts of imaging data. This enables their precise delineation of anatomical structures with minimal human intervention. While atlas-

based segmentation is another explored machine learning-based approach, this model relies on predefined anatomical templates (i.e., atlases) for segmentation (Conroy et al., 2021; Zhou et al., 2019). This is limited compared to deep learning models, which can learn intricate patterns beyond what is explicitly present in atlases, allowing for adaptations to various imaging data and more precise segmentations. Studies have demonstrated up to 15% increases in Dice Similarity Coefficient (DSC) performance of deep learning models compared to atlas-based models for prostate contouring (Balagopal et al., 2021), though not all studies obtain significant performance improvements (Ahn et al., 2019; Conroy et al., 2021; Zhou et al., 2019).

For cancer treatment, the optimization of radiation delivered in treatment planning holds paramount importance. Radiotherapy requires precise and personalized approaches to meet optimal treatment outcomes while minimizing adverse effects on healthy organs and tissues. For newly diagnosed prostate cancer cases, initial management of the disease ranges from active surveillance for low-risk patients to definitive management with surgical resection of the prostate and seminal vesicles (prostatectomy) or definitive radiation therapy (RT). While other forms of treatments such as surgery, hormonal therapy, chemotherapy, and internal radiation in the form of brachytherapy are potential avenues for treatment, only external beam radiotherapy (EBRT) in the form of photon treatments will be discussed and investigated (“NCCN guidelines: prostate cancer (version 3.2024).”).

Over the past decades, intensity-modulated radiation therapy (IMRT) and now volumetric-modulated arc therapy (VMAT) have been commonly used treatment modalities for prostate cancer (Ayuthaya et al., 2023; Fogliata et al., 2019). Intensity modulation enables the delivery of a maximum dose to a desired treatment target while minimizing the dose to surrounding normal tissues. These inverse planning techniques demonstrate good responses to patients with early-stage prostate cancer due to their resultant highly conformal dose distributions spread across multiple treatment beams (Ayuthaya et al., 2023; Cahlon et al., 2008; Teoh et al., 2011). The nature of inverse planning presents an iterative approach of trial-and-error to calculate the dose to the patient to then optimize for an effective tailored plan on a

patient-by-patient basis (Ayuthaya et al., 2023; van Gysen et al., 2020). To add to this, there are complex relationships between the targets and multiple OARs to be considered, limitations in beam arrangements and treatment geometry, and the patient's health conditions to create a series of potential “trade-off” scenarios that can affect the plan's quality. The NCCN guidelines provide recommendations on several treatment regimens for the treatment of prostate cancer with external beam radiation. These include recommendations on hypo-fractionated treatments up to SBRT and conventional hyper-fractionated schemes allowing prescription doses up to 95Gy. However, balancing recommendations and patient-specific conditions requires a depth and breadth of the treatment experience for physicians and planners to navigate (Ayuthaya et al., 2023; Kubo et al., 2019; Yuan et al., 2012).

Data from prior “high quality” plans have been assembled to address the variation present in institutional variations to treatments and planner-by-planner variations. These treatment plan stores serve not only to reference previous treatment parameters that have led to optimal treatment for patients but also to guide planning systems to produce plans of similar quality prospectively (Good et al., 2013; Kaderka et al., 2021). It is from these stores of quality prior treatments that knowledge-based planning (KBP) can aid physicians and planners in improving and minimizing the variation within planning (Fogliata et al., 2019; Moore et al., 2011; Reddy et al., 2010; van Gysen et al., 2020). In a study comparing the average PTV dose of hyper-fractionated prostate treatments, knowledge-based plans resulted in statistically significant lower D2% values ($p < 0.05$) compared to manually planned treatments with slightly lower average rectum and bladder doses (Ayuthaya et al., 2023).

Automated treatment methods have been proposed for other cancer treatment sites beyond prostate cancer, including rectal, cervical, and breast cancers. Conventional 3D conformal techniques and intensity-modulated radiation therapy techniques have been automated for rectal and cervical cancers with the use of rule-based, deep learning, or knowledge-based methods for planning (Huang et al., 2022; Kisling et al., 2019; Rhee et al., 2020). Convolutional neural networks for field aperture prediction and support vector machines

for quality assurance have also been implemented to assure treatment consistency and quality in these sites (Huang et al., 2022; Rhee et al., 2022, 2019). Deep learning and knowledge-based planning methods have been proposed for breast cancer (Fogliata et al., 2022), with mean absolute errors for mean doses below 3% for critical targets and normal tissues (Ahn et al., 2021). These methods, however, focus on a limited scope of contoured treatment scenarios for their respective sites, constraining the potential generalizability of treatment. Therefore, there is a need to investigate a treatment pipeline to understand the possible limits of what can be included in a flexible end-to-end automated solution for photon external beam treatments.

This thesis explores integrating deep learning-based image segmentation techniques with knowledge-based treatment planning for delivering radiation therapy for prostate cancer. Furthermore, this thesis will investigate challenges, limitations, and opportunities associated with implementing deep learning segmentation algorithms in the radiation treatment of prostate cancer, including issues related to data quality, model generalizability, and clinical integration. By addressing these challenges and providing insights into potential patterns and solutions for irradiation of target structures, this research aims to provide a framework for facilitating the adoption of deep learning-based image segmentation techniques in routine clinical practice for prostate cancer, ultimately improving the quality and precision of cancer treatment delivery.

CHAPTER 2: CENTRAL HYPOTHESIS AND SPECIFIC AIMS

Central Hypothesis:

Using DL algorithms coupled with Knowledge-Based Planning approaches, we hypothesize that we can establish a flexible end-to-end prostate cancer treatment pipeline for a wide range of clinical treatment scenarios with a 90% clinical acceptability pass rate.

Specific Aim 1:

Aim: Development of a deep learning auto-contouring workflow for prostate radiotherapy using simulation CT imaging

Hypothesis: We hypothesize that deep learning segmentation models can delineate prostate target structures to 90% clinical acceptability with no more than minor edits.

The work towards Aim 1 is presented in Chapter 3: Automated Contouring System for prostate cancer using deep learning frameworks.

Specific Aim 2:

Aim: End-to-end evaluation of knowledge-based planning models for planning intact, postoperative, and pelvic lymph node prostate treatment scenarios

Hypothesis: We hypothesize that knowledge-based planning models can provide full target coverage for a breadth of prostate treatment scenarios while meeting 90% of clinical dose constraints for clinical acceptability with no more than minor edits

The work towards Aim 2 is presented in Chapter 4: Automated Knowledge-based Planning for Prostate Cancer.

CHAPTER 3: AUTOMATED CONTOURING SYSTEM FOR PROSTATE CANCER USING DEEP LEARNING FRAMEWORKS

Introduction

Prostate cancer remains one of the leading causes of male cancer-related death in developed and developing countries, with over 350,000 deaths worldwide in 2020 (Sung et al., 2021). The effectiveness of contemporary treatment options for prostate cancer remains a top research priority, with increasing interest in radiotherapy outcomes (Beesley et al., 2019; Chen et al., 2017; Hamdy et al., 2016). After the selection of radiotherapy for prostate cancer treatment, treatment planning begins with the delineation of target volumes and surrounding normal tissues using CT images for treatment simulation. Contouring these structures is a time- and resource-intensive task that requires expert knowledge to produce anatomically correct soft tissue boundaries (Baroudi et al., 2023). Therefore, there is a vital need for a comprehensive contouring tool(s) that can aid physicians and dosimetrists in accurately delineating structures, allowing more time for plan development and optimization.

In recent years, automated contouring of these structures with deep learning methods has reduced contouring time and, in some cases, improved the quality of clinical contours (Cha et al., 2021; Gooding et al., 2018; Vaassen et al., 2020). Building on the advantageous experiences of prior works, the deep learning approach implemented in this work is the nnU-Net. nnU-Net is a state-of-the-art deep learning framework designed for the deep learning task of medical image segmentation. nnU-Net is a robust segmentation solution for various anatomical structures and abnormalities in medical images such as MR and CT (Isensee et al., 2021).

The deep learning architecture that serves as the basis for nnU-Nets image segmentation is the popular convolution neural network (CNN) design of the U-Net. However, nnU-Net provides additional enhancements that improve segmentation accuracy and efficiency. These enhancements in architecture and approach allow it to handle unique challenges related to medical imaging data, which include limited annotated samples, class imbalance, and high

inter-patient variability (Isensee et al., 2021). The core components of nnU-Net are the encoder-decoder architecture, skip connections, and automated pre- and post-processing workflow.

The encoder-decoder architecture is the downward and upward paths of the U-Net. The encoder (downward path) gradually reduces the spatial dimensions of the input image while increasing the number of feature maps, capturing hierarchical representations of the input data. The decoder (upward path) then up-samples these features to produce a segmentation map with the exact spatial dimensions as the input image (Comelli et al., 2021; Yu et al., 2022). Skip connections enable the network to access low-level and high-level features at upward path points in the model, facilitating more precise segmentation. These connections preserve the spatial information learned during the dimensionality reduction of unique information in the encoder to prevent the learned weights from input image data from being lost, solving the vanishing gradient problem (Mohammadi et al., 2021).

The pre-and post-processing workflows of nnUnet are centered around extracting domain knowledge from biomedical data. Domain knowledge is the general background knowledge of the data or environment to which the data science methods are applied. It involves analyzing and interpreting the relevant information and features present within the data to enhance predictions. nnU-Net separates this data into three parameter groups: fixed, rule-based, and empirical parameters. The first are fixed parameters, templates from state-of-the-art deep learning model architectures that have proven to work well for various segmentation tasks. The next are rule-based parameters, which establish unique features of your dataset and then formulate the dependencies to process your data for training. To handle object size and shape variations within biomedical imaging data, nnU-Net creates a "dataset fingerprint." This fingerprint consists of non-zero region cropping to evaluate image size, image spacing, number of classes, and intensity values within image and label data. The network can effectively segment structures of different scales by incorporating multiple input data resolutions through spatial resampling. The default resampling technique in nnU-Net is third-

order spline interpolation, which also performs linear or nearest-neighbor interpolation (Isensee et al., 2021). Additionally, intensity normalization and data augmentation are employed to ensure consistent inputs and increase the diversity of training data to improve the segmentation of unseen input images. Finally, empirical parameters refer to selecting the best-trained model and post-processing the results for optimal segmentation. For post-processing, connected component analysis isolates individual regions within the segmentation mask to separate overlapping structures. Morphological operations such as dilation, erosion, and smoothing are also explored on the final segmentation mask to remove minor artifacts and irregularities in the segmentation mask (Isensee et al., 2021).

We have recently demonstrated that deep learning models can reduce treatment planning times by up to 26% compared to manual segmentation (Rhee et al., 2020). Similar model-focused studies have demonstrated that deep learning-based methods can segment tumor volumes and normal tissues with approximately 90% or greater similarity to manually segmented regions by radiation oncologists (Cha et al., 2021; Duan et al., 2022; Kazemifar et al., 2018; Pan et al., 2019). Therefore, it seems likely that advanced deep learning algorithms can delineate tissues on CT images to model delivered radiation accurately. This study proposes that models developed from data trained in the nnU-Net framework can contour prostate treatment planning structures. This auto-segmentation stage is the first stage of the proposed end-to-end treatment pipeline. The inputs for this pipeline are a simulation CT and a radiotherapy prescription with details on the dose and targets to irradiate with desired margins. For auto-segmentation, the input is the simulation CT with information on targets to aid in post-processing only.

Methods

Patient Dataset

Data for developing the automated treatment pipeline was obtained from institutional Pinnacle and RayStation databases. A dataset of 1069 patients' simulation CTs, clinical

contours, IMRT, and VMAT plans were extracted to represent a breadth of clinical treatment scenarios for prostate cancer, including definitive (intact) prostate, post-operative (postop) prostate, and lymph node-involved treatment cases. These cases include treatment devices (i.e., rectal balloons and space-oir hydrogels) and imaging artifacts due to metal hip implants. The extensive collection of prostate cases was selected to enhance the model’s training and make it more robust to unseen cases.

The collected data containing treated patients between 2010 and 2023 was evaluated to ensure that CTs, manual contours, and VMAT treatment plans were clinically approved and used in treatment. Each contour selected for training was assessed individually for observance of guidelines for model training with supervision from a radiation oncologist (see Table 1). Selected clinical contours include the Prostate, Prostate Bed, Seminal Vesicles (SV), SV-fossa, Rectum, Sigmoid, Bladder, Femoral Heads, Hydrogel Spacer, and Rectal Balloon.

Organization	Structures	Reference
ESTRO	Intact Prostate	<i>ESTRO ACROP consensus guideline on CT- and MRI-based target volume delineation for primary radiation therapy of localized prostate cancer</i> (Dal Pra et al., 2023)
RTOG	Post-operative Prostate, Normal Pelvic Tissues	<ul style="list-style-type: none"> • <i>Development of RTOG consensus guidelines for the definition of the clinical target volume for postoperative conformal radiation therapy for prostate cancer</i> (Michalski et al., 2010) • <i>Pelvic Normal Tissue Contouring Guidelines for Radiation Therapy: A Radiation Therapy Oncology Group Consensus Panel Atlas</i> (Gay et al., 2012)
NRG	Pelvic Lymph Nodes	<i>NRG Oncology Updated International Consensus Atlas on Pelvic Lymph Node Volumes for Intact and Postoperative Prostate Cancer</i> (Hall et al., 2021)

Table 1 Summary of contouring guidelines observed to curate ground truth data for deep learning model development.

Some structures necessary for the development of our models were either not contoured for treatment or exhibited high inter-user variability. These include PenileBulb, Bowel Bag, Lymph Node CTV, Cauda-Equina, and Spinal Cord. For PenileBulb, Lymph Node CTV, Cauda-Equina, and Spinal cord, these contours were retrospectively manually contoured by trained research assistants for 100 patients following RTOG Consensus Contouring Guidelines (Gay et al., 2012). Two radiation oncologists reviewed these structures iteratively until they

were correctly contoured according to guidelines. In addition to Lymph Node CTV, the aortic bifurcation, the junction where the abdominal aorta bifurcates into the left and right common iliac arteries, was contoured to ensure the appropriate superior termination of the Lymph Node CTV according to NRG guidelines. The bifurcation was contoured for 15 slices: five below the bifurcation point and ten above. The bifurcation point was set where two distinct ellipses were first visible on CT (see Figure 1). The Lymph Node CTV was contoured three more slices above the superior slice of the aortic bifurcation to ensure that total contour volume at and above the end of the bifurcation was predicted at the superior boundary. For the Bowel Bag and kidneys, contours were automatically generated on the final testing patient sets from deep-learning models developed by our group (Rigaud et al., 2021; Salazar et al., 2024).

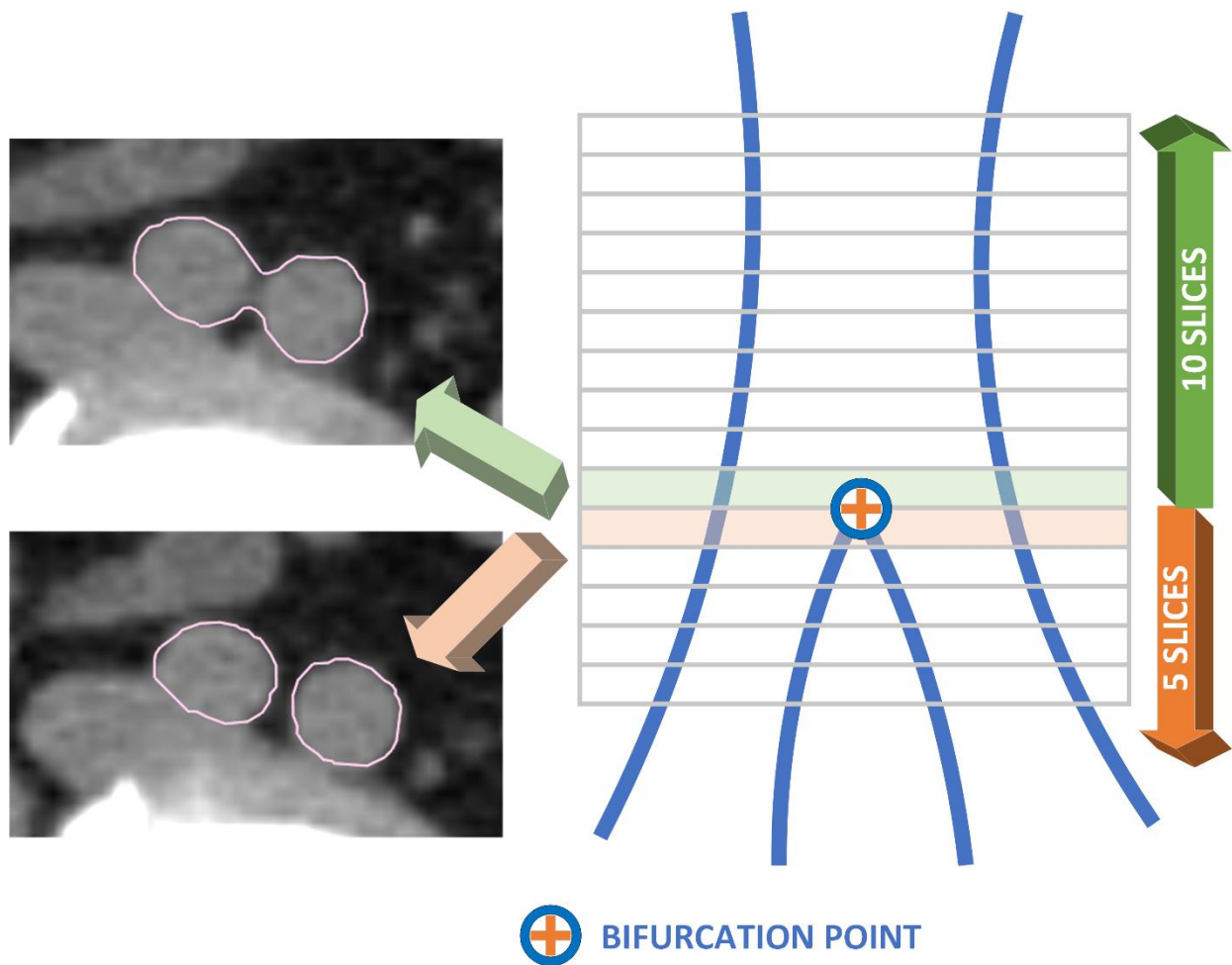


Figure 1 Illustration of contouring the aortic bifurcation as the support structure for lymph node CTV contouring according to NRG guidelines.

Contour Model Development

Preparation of data for contour model training

Five models were developed for the segmentation of all prostate structures. Clinical and non-clinical contour data was separated into specific segmentation map groups for model training: targets, organs-at-risk (OARs), nodal contours, spinal contours, and devices. Intact and postoperative targets (e.g., prostate and seminal vesicles) were combined onto a single segmentation map for multi-class prediction. OARs routinely contoured for prostate treatment planning, including rectum with a rectal balloon, were combined into another segmentation map for multi-class prediction. The same was performed for nodal contours (e.g., Lymph Node CTV and aortic bifurcation) and spinal contours (Cauda-Equina and Spinal Cord). The device segmentation map consists of hydrogel spacer contours only for single-class prediction. If ground truth structures overlapped, a priority order was used to prioritize structures with stringent dose constraints over less stringent ones. The order is prostate, seminal vesicles, rectum, sigmoid, bladder, lymph node CTV, femoral heads, penile bulb, bowel bag, cauda equina, spinal cord, and kidneys from most stringent to least stringent dose constraints. All images were resampled to 1.17mm x 1.17mm pixel size and 2.5 mm slice thickness. Contour data was split into training, fine-tuning, and testing datasets in an 80:10:10 percent split. A complete list of contoured structures can be seen in Table 2.

New Models and Generated Contours					Adopted Model Contours
<i>Pelvic Target Structures</i>	<i>Nodal Structures</i>	<i>Pelvic OARs</i>	<i>Spinal OARs</i>	<i>Devices</i>	<i>Adopted OARs</i>
Prostate Prostate Bed Seminal Vesicles SV-Fossa	Pelvic Lymph Node CTV Aortic Bifurcation	Rectum Rectal Balloon Sigmoid Bladder Penile Bulb	Cauda Equina Spinal cord	Hydrogel Spacer	Bowel Bag (Salazar et al., 2024) Kidneys (Rigaud et al., 2021)

Table 2 Target, organs-at-risk (OARs), and other structures automatically contoured within our treatment pipeline, separated by structures from newly developed models and structures adopted from established models.

Model Training

For each of the five groups of labeled data prepared above, the adaptive nnU-Net framework (Isensee et al., 2021) was used to tailor segmentation models based on 3D U-Net architecture to segment prostate treatment structures. An example architecture of a customized Un-Net architecture can be seen in Figure 2. The loss function for each model was a combination of Dice Similarity Coefficient (DSC) loss and cross-entropy loss. Training and testing were done on NVIDIA Tesla V100 GPUs with 32 GB VRAM. Each model was also trained for 1000 epochs.

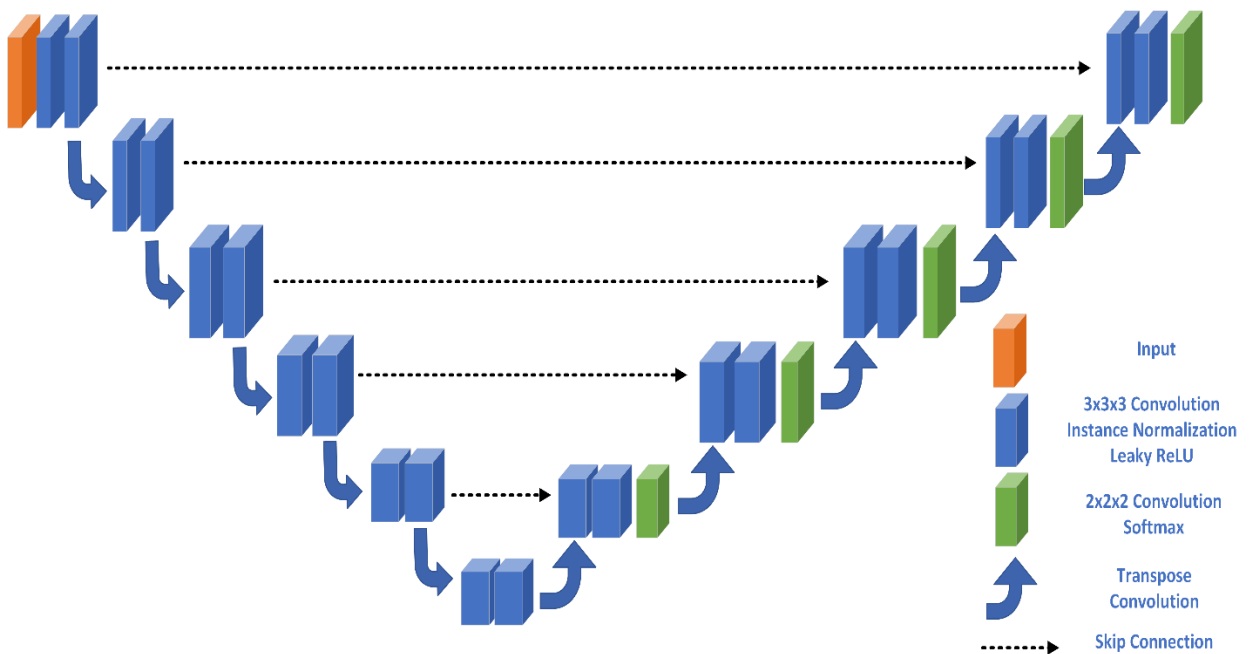


Figure 2 U-Net architecture was customized for the segmentation of structures by the nnU-Net Framework based on available training data.

Out of all the patients' simulation CT scans separated into the training dataset, not all structure labels were drawn on that CT. To obtain a complete set of labeled data from which to train our models, all available clinical contours for specific regions of interest (ROIs) were first used to train treatment case-specific models. Each model was trained using the nnU-Net framework for a particular ROI depending on the treatment scenario in which the contour would be present. The circumscribed features for a given contour and treatment scenario allow the model to learn from these limited, more specific delineations. The predictions from models for

similar treatment cases but distinct segmentation features were summed to improve the generated contours. The deep-learning contour predictions from these models are then combined to create a complete structure set for each training patient in the training dataset. Final targets and OAR models were trained using this deep-learning contour dataset. A Model ID is included as a reference to model outputs summed together for a given treatment scenario to generate a deep learning prediction dataset for the final model (see Table 3 and Figure 3). A paired t-test was performed to examine the difference between the mean geometric metric performance of contours generated from deep learning predictions and contours generated from ground truth clinical data. This was done to support that contours generated from deep learning models did not vary significantly from the predictions of conventionally trained models. Individual, ensemble and the proposed multi-class model were compared for metric performance on Dice-Similarity-Coefficient (DSC) and 95% Hausdorff Distance (HD95) with an alpha level of significance set at 0.05.

Region of Interest	Model ID	Model Description	Treatment Case
Prostate	1	Prostate (intact)	Only treatments with prostate intact
	2	Prostate (postop)	Only prostatectomy cases
	3	Prostate (intact and postop)	All treatment cases
	4	Prostate (with spacer)	Only treatments with hydrogel spacer
Seminal Vesicle	5	Seminal Vesicle (total intact)	Only treatments with intact Seminal Vesicles (proximal SV + distal SV)
	6	Seminal Vesicle Fossa	Only prostatectomy cases
	7	Seminal Vesicle (intact and postop)	All treatment cases
Rectum	8	Rectum (with and without balloon)	All treatment cases with and without rectal balloon present
	9	Rectum (ischial tuberosity)	All treatment cases with rectum extending to or below the ischial tuberosity
Sigmoid	10	Sigmoid (no balloon)	All treatments with sigmoid where no rectal balloon was used
	11	Sigmoid (with balloon)	All treatments with sigmoid where rectal balloon was used
	12	Sigmoid (with and without balloon)	All treatments, regardless of the use of a rectal balloon

Bladder	13	Bladder	All treatment cases
Femoral Heads	14	Femoral Heads	All treatment cases, including the presence of metal hip implants
Penile Bulb	15	Penile Bulb	All treatment cases

Table 3 Summary of contouring models developed on a treatment-case basis.

Only one model was developed for these structure groups: nodal, spinal, and device structures. This is because all contours were present for all training patients after manual contouring was approved. The nnU-Net framework was used to tailor 3D full-resolution U-Nets to our dataset for five new nnU-Net models. Two existing models developed for generating contours for bowel bag and kidneys were incorporated to include a complete set of contours for prostate treatments (a total of 7 models).

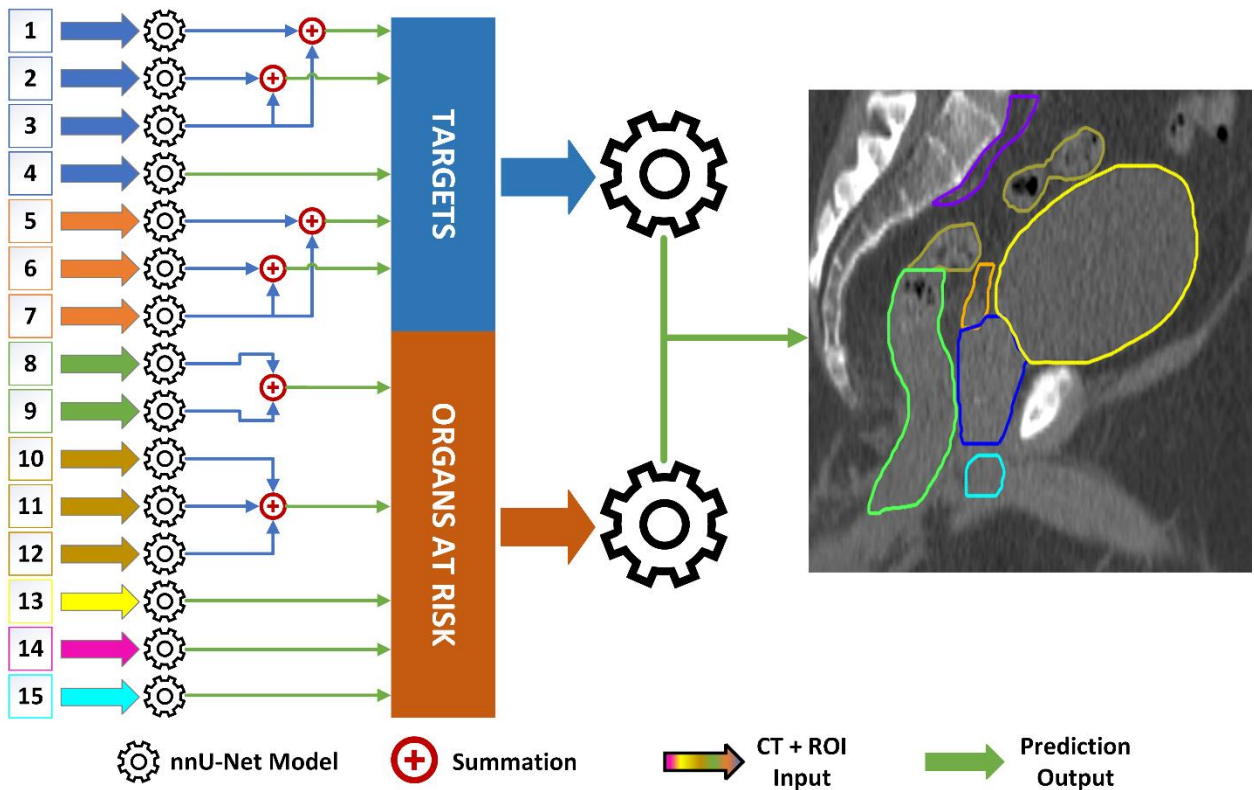


Figure 3 Workflow of combining model predictions from clinical data to create a complete training contour set of deep learning predictions. From the targets and OARs deep learning prediction dataset, the final two targets and OAR nnU-Net models are trained to contour respective structures. The numbering on the left-hand side corresponds to the Model ID in Table 3.

Post Processing

Additional contour corrections were necessary to combine all the predicted structures from various models. The first correction of contours needed was the overlap between

predicted targets and OARs. The order of overlap correction was the same as for pre-processing: prostate, seminal vesicles, rectum, sigmoid, bladder, lymph node CTV, femoral heads, penile bulb, bowel bag, cauda equina, spinal cord, and kidneys. For continuous structures such as Prostate Bed/SV-fossa, Rectum/Sigmoid, and Cauda Equina/Spinal Cord), the boundaries required adjustment to avoid multiple predictions on the same slice axially (see Figure 2). Additionally, a 1.5mm and 1mm anterior and lateral reduction was necessary for the prostate to avoid contouring into the neurovascular bundle surrounding the prostate. For the prostate bed, a similar anterior and superior 1mm and 2mm reduction was required to prevent excessive contouring into the bladder. The middle slice with overlap was chosen for each structure pair as the boundary between ROIs. As the total seminal vesicle volume was contoured, the seminal vesicles were truncated based on the desired treatment extent for intact treatment cases. For example, if the physician indicates they want to treat the proximal 1.5cm, the seminal vesicles are truncated at the 1.5cm point.

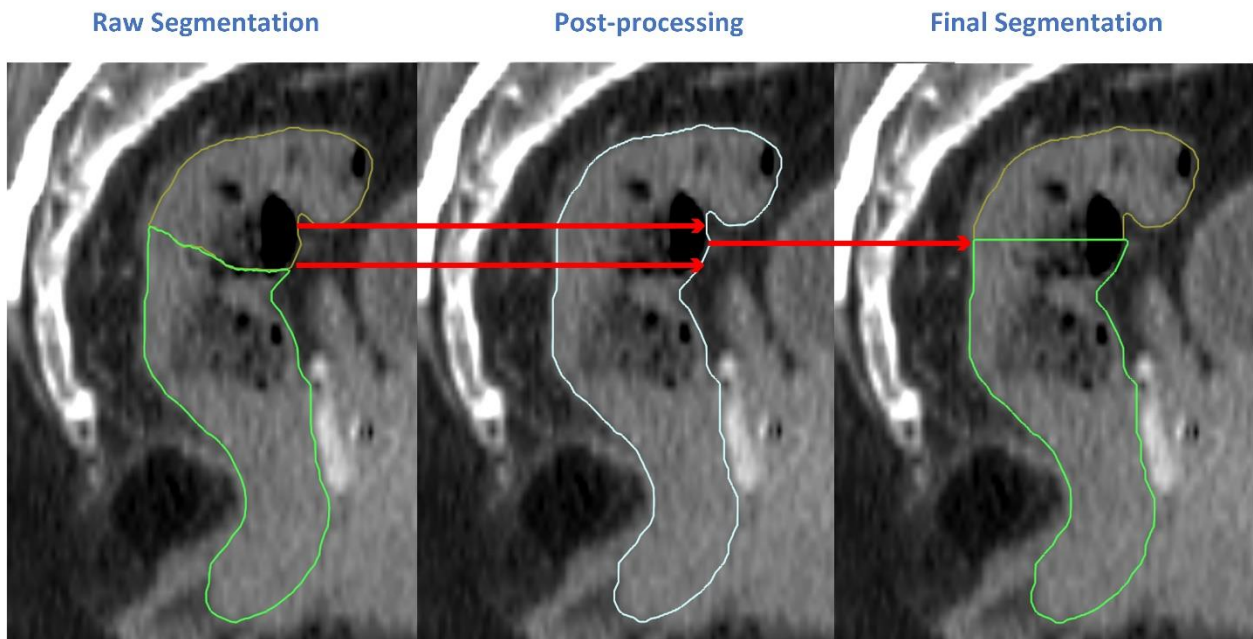


Figure 4 Boundary correction was performed on generated segmentations of model predictions. An example of an auto-contoured rectum and sigmoid prediction being reset to the median overlapping slice from the contour boundaries' most inferior and superior borders.

Contour Evaluation

The final set of model prediction contours was evaluated on the held-out test dataset of 100 patients. The performance of model-generated contours was evaluated using Dice-Similarity-Coefficient (DSC), Surface DSC, 95% Hausdorff Distance (HD95), and mean surface distance (MSD). From the test dataset, 65 patients were selected for physician review of contours (45 and 20 patients without and with lymph node involvement, respectively). Four radiation oncologists from two institutions and two countries visually evaluated and scored the auto-contours on a five-point Likert scale shown in Table 4.

Score	Acceptability	Description
5	<u>Acceptable</u> ; use as is	Clinically acceptable, could be used for treatment without change
4	<u>Acceptable</u> , minor edits that are not necessary	Stylistic differences are not clinically significant; the current contours/plans are acceptable.
3	<u>Unacceptable</u> , minor edits that are necessary	Clinically significant edits, but it is more efficient to edit the automatically generated contours/plans than to start from scratch.
2	<u>Unacceptable</u> , major edits	Edits that are required to ensure appropriate treatment and sufficiently significant that the user would prefer to start from scratch
1	<u>Unacceptable</u> , unusable	Automatically generated contours/plans are so bad that they are unusable (i.e., wrong body area, outside confines of the body, etc.)

Table 4 The table details the 5-point scale for evaluating the quality of generated auto-contours and auto-plans.

Results

Of the final five models trained for this auto-contouring stage of our end-to-end pipeline (see Table 2), the multi-class models for pelvic target and OAR structures were compared against individual and ensemble models for statistical variation in contour performance. In evaluating the performance of the proposed multi-class models against individual and ensemble models, no statistical significance was found in contour segmentation for all structures except for rectum contours. P-values for rectum contour predictions between the ensemble and the proposed multi-class model for OAR structures were 2.7×10^{-11} and 3.3×10^{-11} for DSC and HD95, respectively. An example of the distribution of scores between examined model classes for DSC is presented in Figure 5. Upon visually inspecting these

contours, the variations were within the transition zone between the rectum and sigmoid. As this is a loosely defined transition point in guidelines between continuous structures based on observed curvature, it was decided to proceed with the proposed multi-class OAR model to physician review where this statistical difference in contour predictions could be qualified.

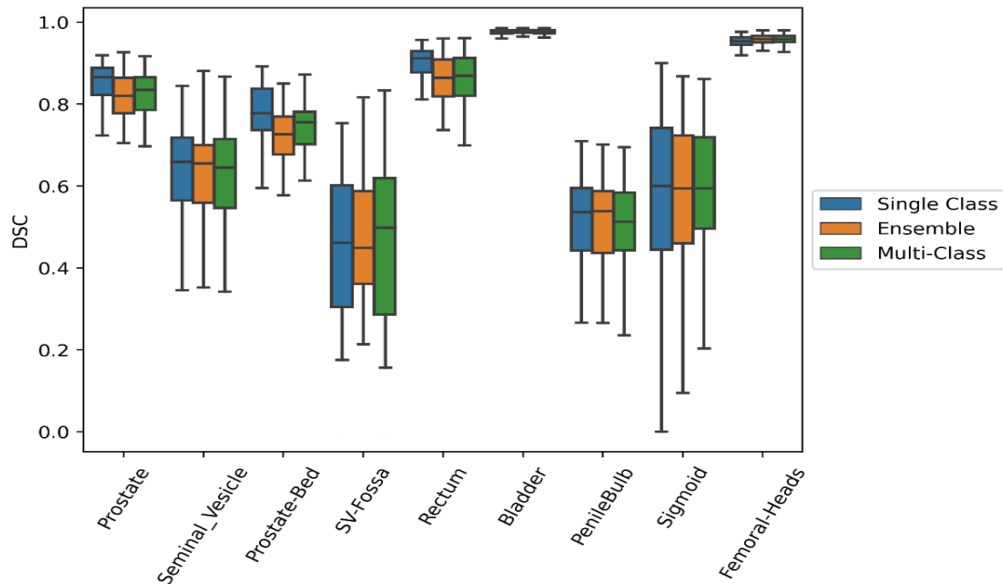


Figure 5 Boxplot of the distribution in DSC scores between predicted structures from individual, ensemble, and the proposed multi-class segmentation models

A summary of the auto-contouring quantitative evaluation for all models is provided in Table 5 for overlap and distance metrics for the 100 test patients in the holdout set. DSC boxplots for all contoured structures are shown in Figure 3. For target structures, prostate, prostate bed, and lymph node CTV achieved the highest mean DSC values at 0.82 ± 0.08 , 0.74 ± 0.07 , and 0.78 ± 0.06 , respectively. More significant variability in auto-segmentation performance was seen in seminal vesicle and SV-Fossa with mean DSC of 0.61 ± 0.17 and 0.58 ± 0.11 , respectively. Variability was attributed to the complex orientations of adjacent organs to seminal vesicles and SV-Fossa (i.e., bladder, rectum, and sigmoid). For distance metrics, prostate, and prostate bed were closely in agreement with HD95/MSD of $7.7 \pm 2.8 / 2.7 \pm 1.0$ and $7.8 \pm 2.9 / 2.8 \pm 1.2$ respectively. Seminal vesicles and SV-Fossa exhibited greater distances of $8.5 \pm 5.8 / 2.6 \pm 2.0$ and $8.4 \pm 4.0 / 3.1 \pm 1.3$. Lymph node CTV presented the greatest target HD95 and MSD of 17.2 ± 20.7 and 3.5 ± 2.7 , respectively.

Most structures achieved a mean DSC value of 0.8 or greater for normal tissue structures, ranging from 0.85 to 0.98. The bladder, kidneys, and femoral heads achieved the highest mean DSC of 0.97 ± 0.02 , 0.98 ± 0.01 , and 0.96 ± 0.02 . For surface DSC, Bladder, Kidneys, and femoral heads, they achieved the highest mean surface DSC of 0.95 ± 0.05 , 0.94 ± 0.03 and 0.98 ± 0.01 . Structures achieving mean DSC values less than 0.8 include Sigmoid, Penile Bulb, and Bowel Bag with mean DSC of 0.63 ± 0.12 , 0.59 ± 0.12 , and 0.68 ± 0.25 , respectively. For surface DSC, Sigmoid, Penile Bulb, and Bowel Bag achieved the lowest mean surface DSC values of 0.78 ± 0.13 , 0.50 ± 0.12 and 0.28 ± 0.18 respectively. For distance metrics, Sigmoid and Bowel Bag achieved the greatest mean HD95/MSD of $27.4\pm 16.2/5.8\pm 4.1$ and $78.4\pm 56.3/21.5\pm 16.6$ respectively.

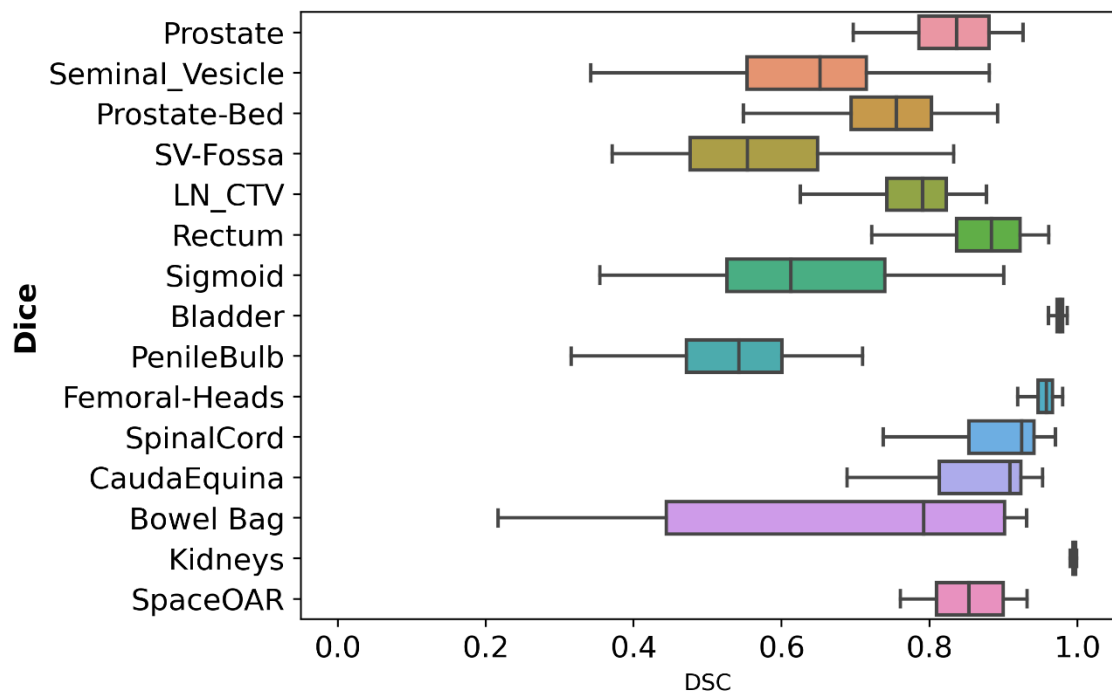


Figure 6 Box and whisker plots of Dice similarity coefficient (DSC) between ground-truth and automatically generated contours.

	DSC		Surface-DSC		HD95 (mm)		MSD (mm)	
	Mean	SD	Mean	SD	Mean	SD	Mean	SD
Prostate	0.82	0.08	0.63	0.18	7.7	2.8	2.7	1.0
Seminal Vesicle	0.61	0.17	0.62	0.18	8.5	5.8	2.6	2.0

Prostate Bed	0.74	0.07	0.46	0.11	7.8	2.9	2.8	1.2
SV-Fossa	0.58	0.11	0.41	0.11	8.4	4.0	3.1	1.3
Lymph Node CTV	0.78	0.06	0.62	0.8	17.2	20.7	3.5	2.7
Rectum	0.85	0.07	0.82	0.09	10.5	8.4	2.0	1.5
Sigmoid	0.63	0.12	0.78	0.13	27.4	16.2	5.8	4.1
Bladder	0.97	0.02	0.95	0.05	2.8	6.0	0.5	1.0
PenileBulb	0.59	0.12	0.50	0.12	9.4	3.5	3.1	1.1
Femoral-Heads	0.96	0.02	0.94	0.03	5.6	5.1	0.8	0.6
Spinal Cord	0.89	0.08	0.90	0.09	15.8	16.9	2.5	2.7
Cauda Equina	0.86	0.10	0.86	0.11	15.1	12.6	2.7	2.2
Spacer	0.85	0.05	0.92	0.07	3.1	2.2	0.8	0.4
Bowel Bag	0.68	0.25	0.38	0.18	78.4	56.3	21.5	16.6
Kidneys	0.98	0.01	0.98	0.01	0.4	0.7	0.1	0.1

Table 5 Mean Dice similarity coefficient (DSC), surface DSC, 95% Hausdorff Distance (HD95), and mean surface distance (MSD) between ground truth and prediction results for our auto-contouring models.

Figures 4 and 5 show the results of the physicians' qualitative evaluations of auto-segmented prostate structures. The contours were separated into two groups to mirror physician review of plans generated from the same set of reviewed contours (i.e., one set of 45 patient cases for prostate without nodal involvement and another set of 20 for prostate cases with nodal involvement).

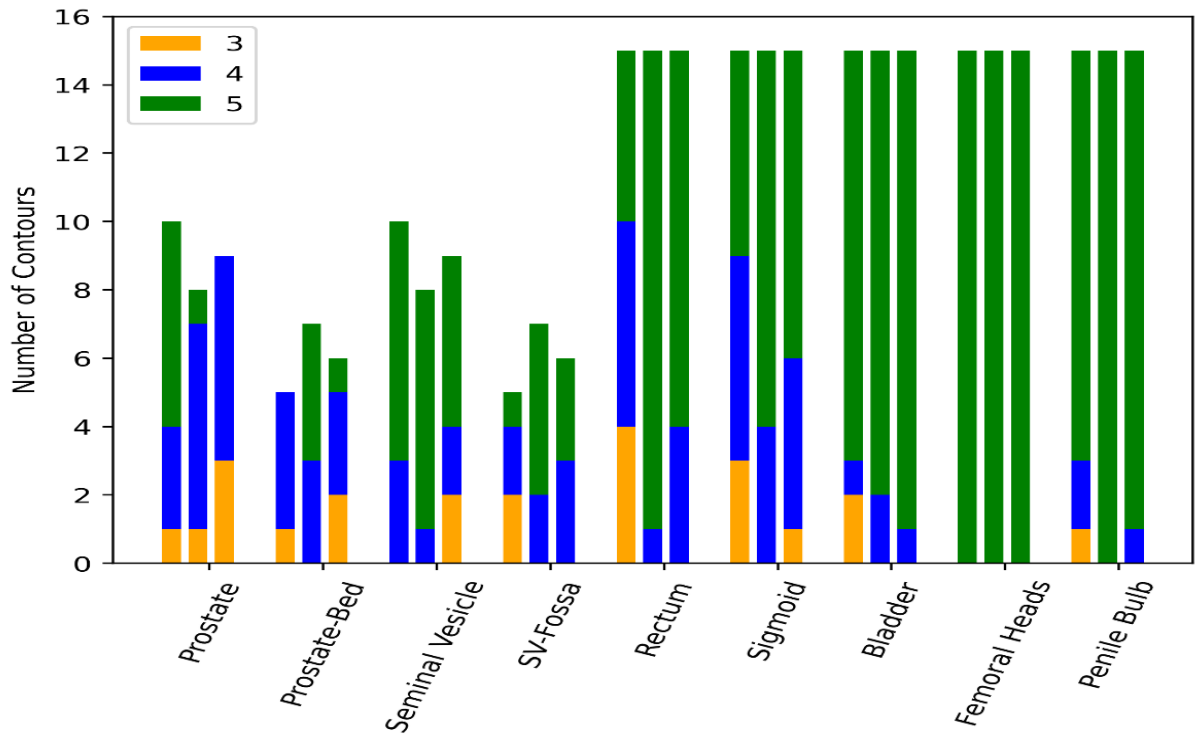


Figure 7 Qualitative review of 45 sets of patient contours on CT by three radiation oncologists for planning structures of intact and postop treatment cases. Each physician reviewed 15 intact and postop cases in total.

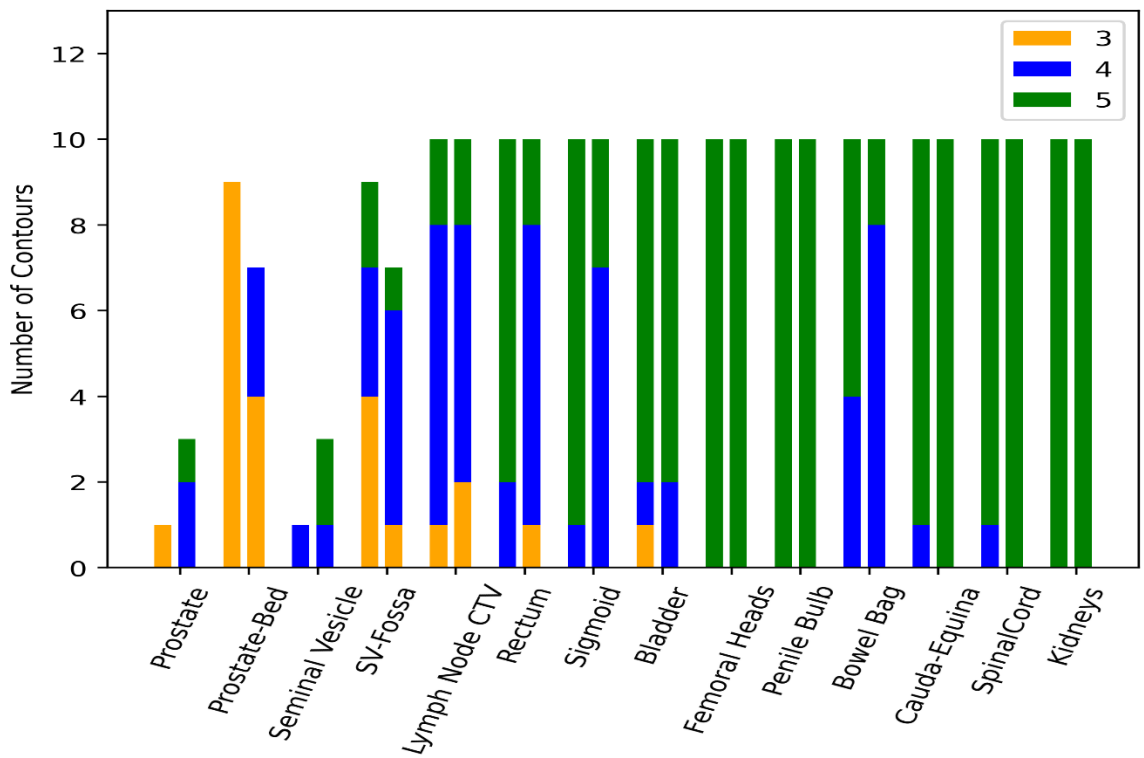


Figure 8 Qualitative review of 20 sets of patient contours on CT by two radiation oncologists for planning structures of intact and postop treatment cases. Each physician reviewed ten intact and postop cases in total.

There was a fair agreement between physician reviewers for contours reviewed in the set of 45 patients. For target structures, physician 1 scored 90% of intact structures and 40% of postoperative structures a 4 or 5. Physician 2 scored 88% of intact structures and 100% of postop structures a four or a five. Physician 3 scores 67% of intact and postop target structures a four or greater. For the rectum, physician 1 scored 73% of contours a 4 or 5. Physicians 2 and 3 both scored all rectal contours a 4 or 5. For sigmoid, physicians 1, 2, and 3 scored their respective evaluated contours a 4 or 5 for 80%, 87%, and 93% of cases. Physicians 2 and 3 scored all bladder and penile bulb contours a 4 or 5. Physician 1 scored bladder and penile bulb contours a 4 or 5 at 87% and 93% of the time, respectively. All physicians scored all Femoral Head contours a 5.

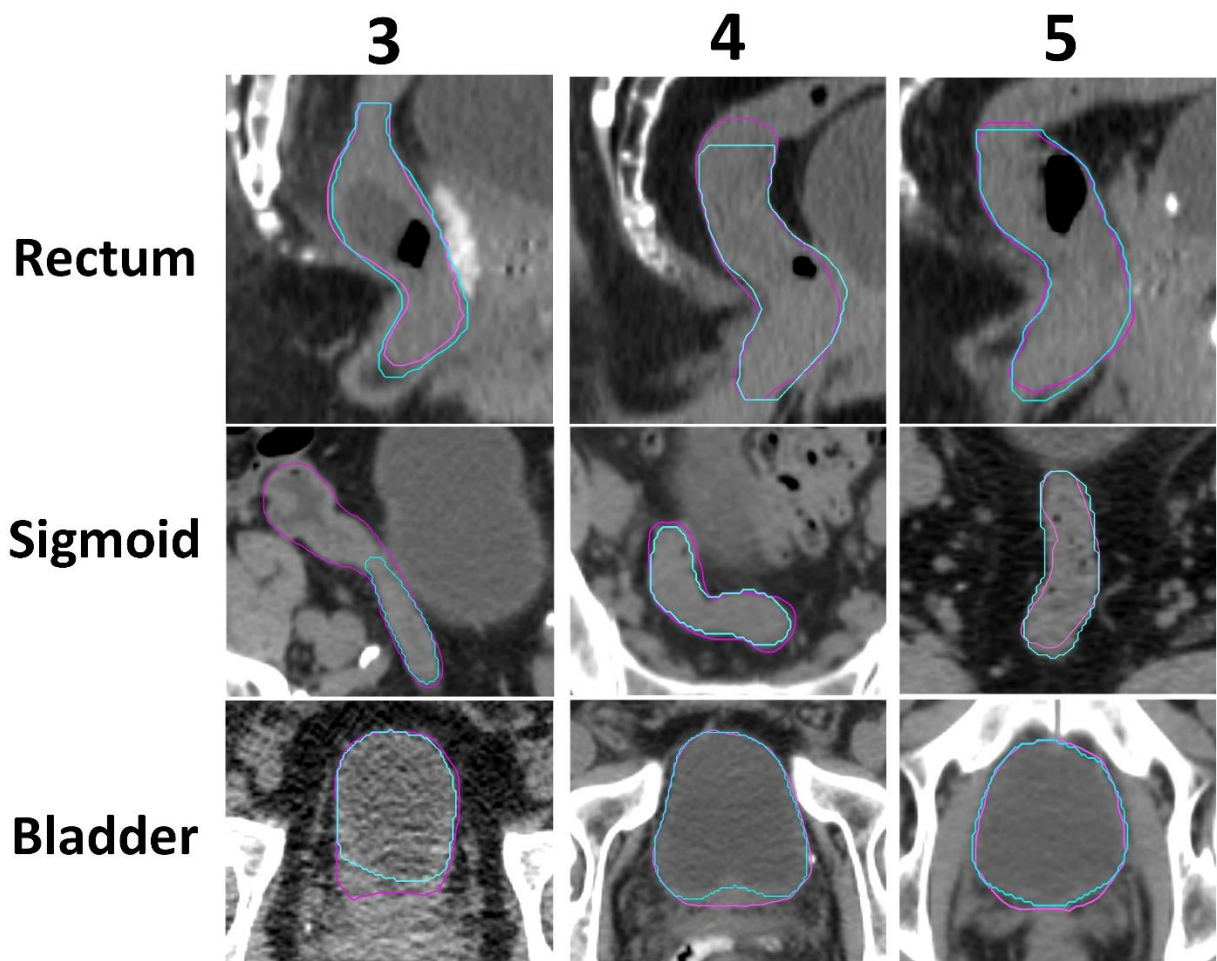


Figure 9 Visual comparison of qualitative physician scoring for predicted contours (cyan) to clinical ground truth contours (magenta) for organs at risk: rectum, sigmoid, and bladder.

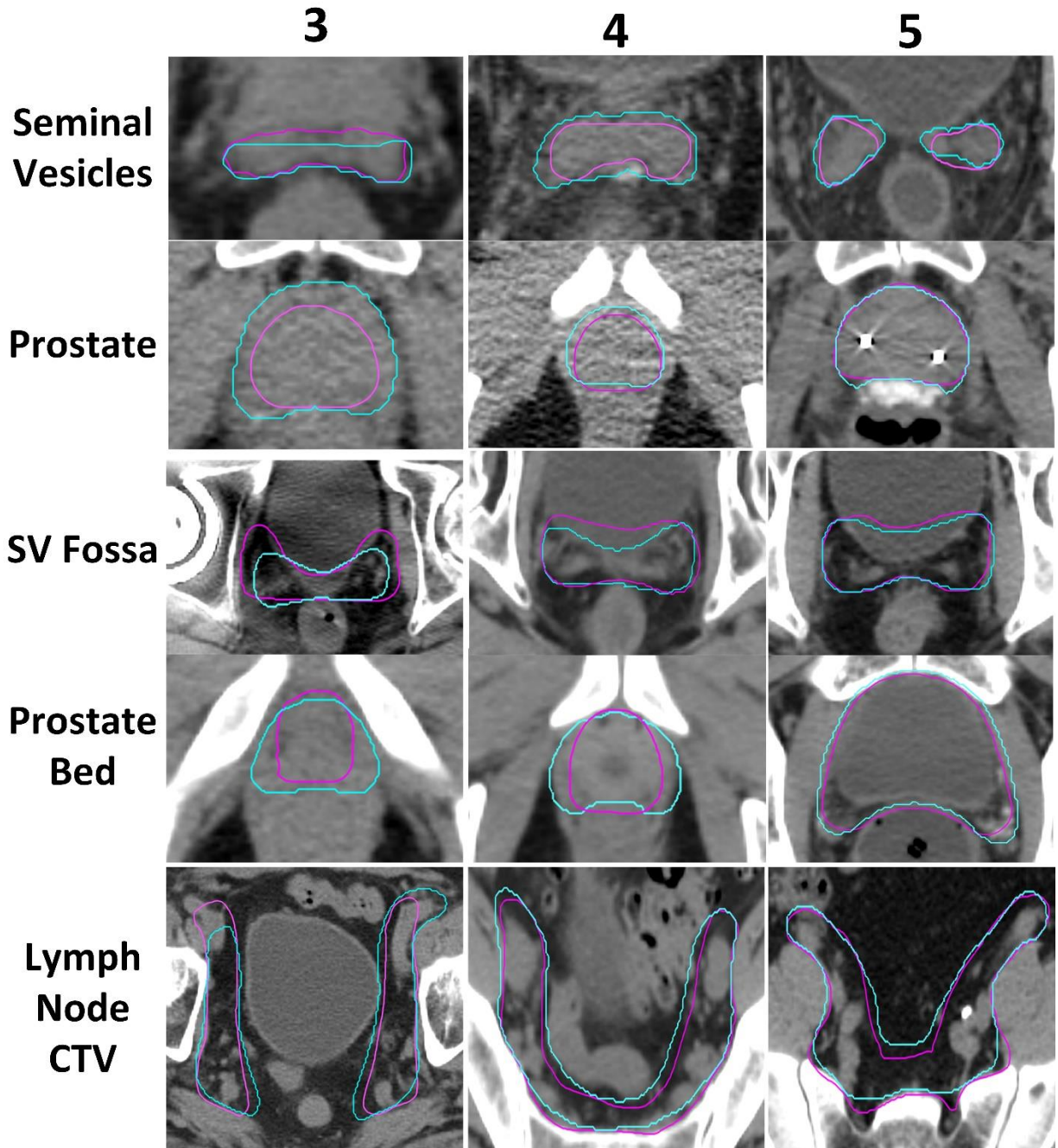


Figure 10 Visual comparison of qualitative physician scoring for predicted contours (cyan) to clinical ground truth contours (magenta) for target structures: prostate, seminal vesicles, prostate bed, SV-fossa, and lymph node CTV.

For contours reviewed in the set of 20 patients, there was a fair agreement between physician scores for OARs and a more varied agreement for targets. For example, for physician 1, the prostate contour reviewed received a score of 3, while the corresponding seminal vesicle structure received a 4. More prostate bed and SV contours were present in this contour set. Physician 1 scored all prostate bed contours a three, and only 56% of SV-Fossa's

scored a 4 or 5. For Physician 2, all prostate and seminal vesicles received a score of 4 or 5. Prostate bed and SV-Fossa contours scored 4 or 5, 43% and 86% of the time, respectively. Both physicians scored Lymph node CTVs as 4 or 5 for at least 80% of cases. The majority of normal tissue structures received either a 4 or 5 for both physicians. Physician 1 scored one bladder contour a three due to incomplete contouring of the bladder neck.

Upon evaluation of the predicted contours that were reviewed to the ground truth clinical contours, differences between lower and higher-scoring contours were made more evident (see Figure 9). For normal tissues, the differences in scoring occurred at the superior and inferior borders. For the rectum, scores of 3 were attributed to over-contouring inferiorly at the level of the anal canal. 4s were mainly attributed to not contouring the superior boundary high enough at the point of the greater curvature of the GI tract. And scores of 5 were able to match these boundaries appropriately. For sigmoid, we see a similar pattern in scoring by the extent of boundaries superiorly. 3s were scored because insufficient sigmoid was contoured superiorly or laterally compared to ground truth. 4s were closer to contouring to the ascending portion of the bowel. 5s could reach and, in some cases, contour more than what was contoured clinically. Bladder scoring centered around the extent of contouring the bladder neck close to the prostate. 3s under contoured this region, segmenting the water within the bladder but not the complete bladder; 4s contoured more of the bladder neck, and 5s could contour the bladder completely.

Scoring in target structures depended primarily on whether the target structure was over or under-predicted. For seminal vesicles, 3s were attributed to under contouring, 4s were often contours that were overextended, contouring more than seminal vesicles in the surrounding (e.g., fat), and 5s were able to contour just the seminal vesicles for the entirety of their length. Prostate 3s were attributed to over-contouring at the middle and apex of the prostate into the neurovascular bundle surrounding the prostate, 4s were slightly contoured, and 5s could adhere to the prostate's visible shape without over-contouring. For postop targets, SV fossa scores were due to contouring, and prostate bed scores were primarily due to over-contouring

into the surrounding obturator and levator ani muscles from scores of 3 to 5, not over-contouring, respectively. For lymph node CTV, lower scores of 3 were due to poor coverage around the iliac blood vessels (see Figure 10). Contours with higher scores could maintain proper margins throughout the body of the lymph node regions.

Discussion

This study aimed to evaluate the ability of trained deep-learning models to delineate both intact and postoperative structures for use in the clinic. Quantitative comparisons for mean DSC and HD95 values to literature are listed in Table 6. As postoperative CTV for prostate may include resected seminal vesicle beds at other institutions, no direct comparison for SV fossa was found for auto-contouring methods. A similar scenario arises for Cauda-Equina, a spinal cord substructure often included as a single contour. For the set of 45 patients, there was more agreement for target structures between physicians 1 and 2 than for those reviewed by physician 3. For normal tissues, there was more agreement between physicians 2 and 3. For the set of 20 patients, there was a more varied response to targets and normal tissues. The inter-observer variability in targets and OARs is similar to studies at multiple centers evaluating three or more physician responses (Kiljunen et al., 2020). A single institution study found that 65% of both prostate targets and OARs (n=43) were acceptable with no more than minor edits using a 3-point scale (Cha et al., 2021). The choice of the Likert scale used to review contours was based on established use in literature for use in automated contouring approaches (Baroudi et al., 2023; Yu et al., 2022). The advantage of a distinction in minor edits with more categories for scoring is in differentiating between contours that are readily acceptable from contours that, although they contain minor edits, would benefit from additional review and redress before proceeding to plan. No physician found that the presented contours needed more than minor edits. When asked about the overall prediction quality, all physicians' feedback was positive, and they were open to future use of these models once they had improved.

Structure	Auto-Contour Mean DSC	Literature Mean DSC	Auto-Contour Mean HD95 (mm)	Literature Mean HD95 (mm)	Reference
Prostate	0.82	0.82	7.7	6.1	(Kiljunen et al., 2020)
		0.87		*4.3	(Oktay et al., 2020)
		0.87		9.9	(Martínez et al., 2014)
		0.86		4.6	(Zabel et al., 2021)
Seminal Vesicles	0.73	0.72	7.5	7.1	(Kiljunen et al., 2020)
		0.8		*3.7	(Oktay et al., 2020)
Prostate Bed	0.74	0.86	7.8		(Balagopal et al., 2018)
		0.65			(Hwee et al., 2011)
SV-Fossa	0.58	**	8.4	**	
Lymph Node CTV	0.78	0.8	17.2	14.7	(Kiljunen et al., 2020)
Rectum	0.85	0.84	10.5	11.4	(Kiljunen et al., 2020)
		0.82		13.52	(Martínez et al., 2014)
		0.84		10.7	(Zabel et al., 2021)
		0.77		6.0	
Bladder	0.97	0.93	2.8	3.3	(Kiljunen et al., 2020)
		0.95			(Balagopal et al., 2018)
		0.89		25.0	(Martínez et al., 2014)
		0.97		2.4	(Zabel et al., 2021)
Femoral Heads	0.96	0.69	5.6	24.8	(Kiljunen et al., 2020)
		0.96			(Balagopal et al., 2018)
		0.98		*1.2	(Oktay et al., 2020)
		0.89		1.4	(Liu et al., 2020)
Penile Bulb	0.59	0.51	9.4	7.7	(Kiljunen et al., 2020)
		0.77			(Balagopal et al., 2018)
		0.6			(Hwee et al., 2011)
Sigmoid	0.63	0.66	27.4	15.3	(Kiljunen et al., 2020)
Spinal Cord	0.89	0.83	15.8	5.01	(Liu et al., 2020)

Cauda-Equina	0.86	**	15.1	**	
Bowel Bag	0.68	0.82	78.4	5.6	(Liu et al., 2020)
Spacer	0.85	0.84	3.1		(Wang et al., 2023)

*Table 6 Comparison of deep learning model segmentation performance to other CT-based contour prediction models in the literature. * Reference reported Hausdorff Distance rather than HD95; ** Structure is not explicitly segmented or is considered part of a larger structure.*

During the contour review, several minor edit recommendations proved to be recurring despite no physician reviewing the same case. For target structures, both prostate and prostate bed suffered from over-contouring. For the prostate, it was most notable at the base and throughout the middle of the prostate. The contours would overextend to contour part of the neurovascular bundle surrounding the prostate. This is difficult to overcome on CT as there is limited soft tissue contrast to differentiate the tissue differences. The presence of metal hip artifacts within our test cases made this distinction of soft tissues problematic, especially in cases that scored 3 for both the prostate and bladder. For the prostate bed, this occurred at the inferior portion of the contour below the anastomosis, following down the obturator and levator ani muscles, which can be challenging to differentiate on CT, depending on quality. The prostate bed auto-contour would contour parts of this muscle inside the CTV, which would not contain unresected tumor cells. Low soft tissue contrast was a recurring issue for cases scoring a 3 for both intact and postoperative prostate. Some physicians deemed it adequate to include some parts of these muscles within the CTV volume. However, physicians noted it is better practice to contour on the innermost boundary of visible pelvic floor muscles or to adjust PTV margins to account for greater uncertainty in the prostate bed contour where appropriate. All reviewers noted potential boundary improvements to the prostate CTV extension into adjacent structures for at least one patient within the review.

Improving coverage of internal iliac vessels for lymph node CTV proved to be a minor but necessary edit. However, the model suffered from the partial volume effect of these vessels caused by proximity to the bowel. Additional information, such as partial contours of these blood vessels, would be needed to ensure the model can adequately capture these structures

without confusion with the surrounding bowel. An example of a partial contour would be the aortic bifurcation contour used in our methods to mark the superior boundary of the Lymph nodes according to guidelines. The added information of this structure significantly improved the model's superior coverage.

For normal tissue structures, the most consistent recommendation was to improve the rectum and sigmoid boundary, most notably when the rectum ends and the sigmoid starts moving upward into the abdomen. This boundary is defined in guidelines as when the GI tract begins to curve upward (Gay et al., 2012). Reference bony anatomy is around the level of S3 or S2. However, within available clinical data, there is significant variation at which this point is defined, resulting in the model often setting the boundary lower for the rectum as the region of curvature varies from patient to patient. This variability inevitably results in the model's difficulty in setting the rectum boundary higher at the point where the most significant curvature between the rectum and sigmoid begins rather than in the middle or end of the curved section. Even the reference bony anatomy of the sacral vertebra is limited depending on sacral curvature and pelvic tilt. Excessive curvature and gas presented within the sigmoid and rectum led the model to over-contour sigmoid and under-contour rectum in cases scoring a three among physicians. Similar difficulties in rectum contouring have been observed for inconsistencies in large datasets (Elisabeth Olsson et al., 2022).

Conclusion

The study proposed, implemented, and tested an automated solution to contour prostate radiotherapy treatment structures. The study demonstrated the clinical acceptability of intact and postoperative structures across two cohorts, with most physicians scoring treatment targets and normal tissue structures with no more than minor edits. Limiting cases of low soft tissue contrast or contents in the bowel are areas of model improvement to reach the desired threshold of clinical acceptability. Each model can segment a breadth of treatment structures

with only one simulation CT as input. This study demonstrates the potential for automated contouring of prostate structures for expedited delineation in preparation for planning.

CHAPTER 4: AUTOMATED KNOWLEDGE-BASED PLANNING FOR PROSTATE CANCER

Introduction

For cancer treatment, the optimization of radiation delivered in treatment planning holds paramount importance. Prostate cancer is one of the most prevalent malignancies affecting men worldwide (Sung et al., 2021), demands precise and personalized approaches to meet optimal treatment outcomes while minimizing adverse effects on healthy organs and tissues. For newly diagnosed prostate cancer cases, initial management of the disease ranges from active surveillance for low-risk patients to definitive management with surgical resection of the prostate and seminal vesicles (prostatectomy) or definitive radiation therapy (RT). While other forms of treatments such as surgery, hormonal therapy, chemotherapy, and internal radiation in the form of brachytherapy are potential avenues for treatment, only external beam radiotherapy (EBRT) in the form of photon treatments will be discussed and investigated (“NCCN guidelines: prostate cancer (version 3.2024).”).

Volumetric modulated arc therapy (VMAT) is now a standard treatment technique used for the treatment of prostate cancer, representing a significant advancement in radiation oncology, offering enhanced dose conformity and sparing of organs at risk compared to conventional conformal approaches (Ayuthaya et al., 2023; Orton et al., 2008). VMAT planning carries a disadvantage in that the optimization process is time-consuming and requires the iterative task of finding the desired target and OAR treatment criteria. Furthermore, an achievable dose-volume histogram is unknown from the start, and optimization parameters are often population-based dose constraints found in previous literature, such as the Quantitative Analyses of Normal Tissue Effects in the Clinic (Marks et al., 2010). Automated knowledge-based planning (KBP) is an increasingly prevalent strategy to expedite and create uniformity in treatment planning, leveraging computational algorithms and large datasets to streamline the treatment planning process (Ayuthaya et al., 2023).

KBP is a technique that leverages the collective information of previous treatment plans to inform and guide the optimization of new plans. This approach utilizes machine learning algorithms to analyze historical treatment data, including dose-volume histogram (DVH) parameters, patient anatomy, and treatment goals, to generate predictive models (van Gysen et al., 2020). These models capture the relationships between various planning parameters and their impact on treatment plan quality. Planning features include patient anatomical features and their relationship to OAR dose-sparing (Yuan et al., 2012). RapidPlan is a commercial knowledge-based planning (KBP) algorithm designed by Varian Medical Systems to streamline the planning process and enhance treatment outcomes. The knowledge base and optimization engine serve as the two key components of this KBP system. The knowledge base is the repository of historical treatment data encompassing a wide range of patient cases and corresponding treatment plans. Studies continue to study the importance of this knowledge base, including the intra- and extra-institutional sources from which the prior treatment data originates for effective and efficient planning (Fogliata et al., 2019; Kaderka et al., 2021; Kubo et al., 2019; Reid, 2019; Zhu et al., 2011). This knowledge base serves as the foundation of the RapidPlans Dose volume Histogram (DVH) estimation. DVHs represent the distribution of radiation dose delivered throughout the treatment volume and are essential for evaluating the quality of a plan by ensuring that dose constraints are achieved. DVH estimation first requires the selection of relevant anatomical structures, which include target volume(s) to be treated and normal tissues to be spared (Moore et al., 2015, 2011; Wu et al., 2009). From the selected structures, statistical regression techniques are used to generate a predictive model (e.g., linear regression) that correlates the geometric and dosimetric features of the patient's anatomy with the estimated DVHs. This model accounts for factors such as tumor size, location, proximity to critical structures, and historical treatment outcomes obtained from the knowledge base. The predictive DVH model is then used to guide the optimization engine by using the DVH to adjust treatment parameters to achieve the desired dose-volume goals iteratively (Li et al., 2021; Zarepisheh et al., 2014). This iterative process enables RapidPlan to

generate high-quality treatment plans efficiently, significantly reducing the time and effort required for manual planning while improving plan consistency and quality.

Knowledge-based planning systems like RapidPlan represent a transformative approach to radiotherapy planning, leveraging historical treatment data and DVH estimation to optimize treatment plans effectively. RapidPlan enables clinicians and dosimetrists to generate high-quality plans tailored to each patient's unique anatomy and treatment objectives, ultimately improving the efficacy of treatment planning while meeting PTV coverage with comparable or improved OAR dose-sparing (van Gysen et al., 2020). Many institutions have begun implementing RapidPlan models into their clinical practice (Ge and Wu, 2019), allowing for reductions in optimization time independent of the planner's skill and planning experience (Kubo et al., 2017). In this study, we propose using two RapidPlan models to generate VMAT plans for intact and postoperative targets with and without lymph node involvement.

Methods

VMAT plan data

Knowledge-based planning models were separately developed for this study to achieve the objective of generating prostate plans. The knowledge base for these Varian RapidPlan models was VMAT treatment plans collected from the most recent year of our cohort (e.g., 2022) to ensure the treatment practices were the most up-to-date in clinical practice. The two cohorts of treatment plans were queried for developing two RapidPlan models. Group 1 consists of 90 intact and postop prostate plans without nodal involvement. Group 2 consists of 37 intact/postop prostate plans with elective pelvic lymph node involvement (both node-positive and node-negative disease). All prostate plans were approved and delivered at a single institution and de-identified under a protocol approved by The University of Texas MD Anderson Cancer Center institutional review board. The institution in which these patients underwent radiotherapy has a dedicated multidisciplinary team of physicians and dosimetrists who specialize in the treatment of prostate cancer. Auto-plans were generated based on the

original physician-drawn and approved targets and normal tissue contours used during treatment.

Automated Planning Strategy

The two previously developed Varian RapidPlan models for automated treatment planning were used for groups 1 and 2 mentioned above. All plans for model development were clinical plans treated from 60 to 78Gy in 20 to 39 fractions for prostate-only cases and 59.8 to 70Gy in 35 fractions for prostate and node cases. All treatments were planned with the Varian Eclipse treatment planning system (version 15.6, Varian Oncology Systems, Palo Alto, CA, USA). All treatment plans consist of three 360° coplanar treatment arcs with a photon energy of 6MV and collimator rotation angles of 10°, 90° and 350°. For prostate-only treatments, the treatment isocenter is set at the center of the prostate PTV. Jaws are set such that the entire target remains in the beam's eye view of the gantry throughout the whole sweep of the arc. The treatment isocenter is set at the center of the combined prostate and lymph node PTV for prostate and lymph node treatments. Jaws are set such that beams of collimator angles 10° and 350° span the combined target PTVs with the beam of collimator angle 90° set to a field size of 15cm around the treatment isocenter (5cm superiorly and 10cm inferiorly).

An automated two-step process was developed to refine the treatment. The specifics of this technique depend on whether the pelvic nodes are to be treated. Two successive optimization iterations are performed after the initial plan is generated to optimize automated treatment plans without nodal involvement. Isodose planning structures are generated from the 105% and 104% isodose lines and progressively added to identify and reduce plan hotspots. This is performed for both intact and postop treatment plans. An isodose planning structure is generated from the 50.4 Gy isodose line to optimize automated treatment plans with nodal involvement. This structure is then used to subtract the isodose planning structure from the original Lymph node PTV volume. The remaining structure, which contains the under-covered regions of the nodal PTV, is used in an additional optimization run to enhance nodal coverage.

All automated treatment plans were normalized such that 98% of the high-risk PTV volume received 100% of the prescription dose.

<u>Target and Normal Tissue Structure</u>	<u>Intact Dose Constraints</u>	<u>Postop Dose Constraints</u>	<u>Lymph Node Dose Constraints</u>
PTV	V78Gy \geq 98% Dose [Max] \leq 84.2Gy	V70Gy \geq 98% Dose [Max] \leq 75.6Gy	V70Gy \geq 98% Dose [Max] \leq 75.6Gy
PTV Lymph Nodes			V50.4Gy \geq 98%
CTV	V78Gy \geq 100%	V70Gy \geq 100%	V70Gy \geq 100%
CTV Lymph Nodes			V50.4Gy \geq 100%
Bladder	V60Gy \leq 40% V70Gy \leq 20%	V60Gy \leq 40% V70Gy \leq 20%	V45Gy \leq 45% V55Gy \leq 25% V65Gy \leq 15%
Rectum	V30Gy \leq 80% V40Gy \leq 60% V60Gy \leq 40% V70Gy \leq 20% (No Balloon) V70Gy \leq 15% (Balloon) V76Gy \leq 15% V 80Gy \leq 5%	V30Gy \leq 80% V40Gy \leq 60% V60Gy \leq 40% V70Gy \leq 15%	
Spinal Cord/Cauda Equina			Dose [Max] \leq 54Gy
Bowel Bag			Dose [Max] \leq 54Gy
Femoral Heads		V50Gy \leq 10% Dose [Max] \leq 50Gy	
Sigmoid		Dose [Max] \leq 60Gy	
Penile Bulb		Dose [Mean] \leq 54Gy	

Table 7 Prostate and Pelvic Lymph node target and normal tissue clinical treatment planning goals.

Auto-Plan Evaluation

To evaluate the performance of the developed RapidPlan models, 40 plans were generated for various radiotherapy prescriptions for prostate, seminal vesicle, and lymph node targets at our institution. Three prescriptions were chosen for intact prostate cases treating prostate and proximal SV with a 6mm uniform and 4mm posterior margin. One prescription was selected for postoperative cases treating prostate bed and SV-Fossa with a 6mm uniform and 4mm posterior margin. Two prescriptions were chosen for nodal-involved cases: the prostate and SV target was applied with a 6mm uniform and 4mm posterior margin, and the lymph node

CTV with a 5mm uniform. A complete list of prescriptions and number of cases evaluated per prescription is shown in Table 8. The resultant auto-plans were quantitatively assessed using clinical target and OAR dose constraints to ensure they met institutional standards. After the plans were generated and normalized, two radiation oncologists reviewed all 40 plans, each evaluating the auto-plans on a five-point scale (see Table 4).

End-to-End Evaluation

To evaluate the performance of the developed end-to-end automated treatment planning process, 65 patients (45 without nodal treatment and 20 with treated nodes) were automatically planned to use auto-contoured treatment targets and normal tissue structures. The entire prostate and the prescribed extent of proximal SV with a 6mm uniform and 4mm posterior margin were treated to 7800cGy in 39 fractions for intact cases. For postop cases, the resected prostate bed and SV-fossa volumes with a 6mm uniform and 4mm posterior margin were treated to 70Gy in 35 fractions. For nodal-involved cases, the prostate/seminal vesicle target with a 6mm uniform and 4mm posterior margin was treated to 70Gy, and the Lymph Node target with a 5mm uniform margin was treated to 50.4Gy in 35 fractions. The resultant auto-plans were quantitatively evaluated using clinical target and OAR dose constraints and compared against the clinical target and OAR contours on the same dose distribution. To inspect the differences between auto-contours and the compared clinical contours meeting or not meeting dose constraints, structures were categorized into meeting, within 5% or greater than 5% of dose constraints. Three radiation oncologists reviewed the auto-plans from auto-contours on a five-point scale (see Table 4). Table 7 shows the planning goals for respective intact-only, postop-only, and nodal treatments. As the second stage of the proposed treatment pipeline, only the auto-contoured structures and radiotherapy prescriptions serve as input. The margins are automatically added to detailed targets within the provided prescription.

Results

Model Evaluation

A summary of the quantitative evaluation of clinical dose constraints on auto-plans generated from manual contours is listed in Table 9 and Table 10. All cases fall within 5% of constraints, with the majority meeting constraints for normal tissues and targets except for 3 cases. One case occurs with the prostate-only model on the high dose constraint for the bladder ($V70Gy \leq 25\%$) in which the bladder descends considerably into the resected prostate bed. Two cases occur within the prostate and node model in which the bowel bag max dose is exceeded by 3Gy, and in another case, the bladder low dose constraint ($V45Gy \leq 45\%$) is exceeded by 8%. In both cases, the respective normal tissues come into close proximity to a large area of the target CTVs.

A total of 40 plans were reviewed by two radiation oncologists for qualitative evaluation of the auto-plans, with scores listed in Table 8. For both oncologists, 95% of the plans scored a four or a five. Of the plans that scored a 3 for the prostate RapidPlan model, physician 1 noted that the PTV coverage could be improved inferiorly and superiorly. Physician 2 indicated that the dose to the bladder could be pushed lower to spare more of the normal tissue for a postoperative case. Of the plans that scored a 3 for the prostate and node RapidPlan model, physician 2 noted that the dose received to the rectum and sigmoid was too high. The sigmoid dose could be made cooler, and the hotspots should be pushed off the lateral walls of the rectum. In general, both physicians approved most plans. Still, they commented that the plans could have improved inferior PTV coverage for the prostate and that the rectum doses along the anterior wall of the rectum could be slightly improved. For the prostate model, the hotspots should be improved around the bladder. For the prostate and node model, the hotspots could be improved in and around the bladder, sigmoid, and bowel.

RapidPlan Model	Prescription	No. Cases	Physician 1 Score			Physician 2 Score		
			3	4	5	3	4	5
Prostate	78 Gy in 39 fractions	10	1	2	7	0	0	10
Prostate	72 Gy in 30 fractions	1	0	0	1	0	1	0
Prostate	70 Gy in 35 fractions	6	1	4	1	1	0	5
Prostate	60 Gy in 20 fractions	3	0	1	2	0	1	2
Prostate + Nodes	70 & 50.4 Gy in 35 fractions	16	0	9	7	1	12	3
Prostate + Nodes	59.8 & 46 Gy in 35 fractions	4	0	1	3	0	3	1

Table 8 Qualitative scoring of physician review prostate only and prostate & nodes RapidPlan VMAT treatment plans.

Structure	Constraint	No Cases	Manual Contour, No. (%)		
			<u>Met</u>	<u>Within 5%</u>	<u>Greater than 5%</u>
CTV	V78Gy>=100	10	8 (80)	2 (20)	0 (0)
CTV	V78Gy>=95	10	10 (100)	0 (0)	0 (0)
PTV	V78Gy>=98	10	10 (100)	0 (0)	0 (0)
PTV	V78Gy>=95	10	10 (100)	0 (0)	0 (0)
PTV	$D_{max} \leq 84.2$ Gy	10	9 (90)	1 (10)	0 (0)
CTV	V70Gy>=100	6	4 (67)	2 (33)	0 (0)
CTV	V70Gy>=95	6	6 (100)	0 (0)	0 (0)
PTV	V70Gy>=98	6	5 (83)	1 (17)	0 (0)
PTV	V70Gy>=95	6	6 (100)	0 (0)	0 (0)
PTV	$D_{max} \leq 75.6$	6	5 (83)	1 (17)	0 (0)
CTV	V60Gy>=100	3	3 (100)	0 (0)	0 (0)
CTV	V60Gy>=95	3	3 (100)	0 (0)	0 (0)
PTV	V60Gy>=98	3	3 (100)	0 (0)	0 (0)
PTV	V60Gy>=95	3	3 (100)	0 (0)	0 (0)
PTV	$D_{max} \leq 64.8$	3	3 (100)	0 (0)	0 (0)
CTV	V72Gy>=100	1	1 (100)	0 (0)	0 (0)
CTV	V72Gy>=95	1	1 (100)	0 (0)	0 (0)
PTV	V72Gy>=98	1	1 (100)	0 (0)	0 (0)
PTV	V72Gy>=95	1	1 (100)	0 (0)	0 (0)
PTV	$D_{max} \leq 77.76$	1	1 (100)	0 (0)	0 (0)
Rectum	V30Gy<=80	16	16 (100)	0 (0)	0 (0)
Rectum	V40Gy<=60	16	16 (100)	0 (0)	0 (0)
Rectum	V60Gy<=40	10	10 (100)	0 (0)	0 (0)
Rectum	V70Gy<=20	10	10 (100)	0 (0)	0 (0)
Rectum	V70Gy<=15	16	16 (100)	0 (0)	0 (0)

Rectum	V76Gy<=15	10	10 (100)	0 (0)	0 (0)
Rectum	V80Gy<=5	10	10 (100)	0 (0)	0 (0)
Rectum	V25Gy<=80	1	1 (100)	0 (0)	0 (0)
Rectum	V35Gy<=60	1	1 (100)	0 (0)	0 (0)
Rectum	V50Gy<=40	7	7 (100)	0 (0)	0 (0)
Rectum	V60Gy<=20	1	1 (100)	0 (0)	0 (0)
Rectum	V60Gy<=15	4	4 (100)	0 (0)	0 (0)
Rectum	V65Gy<=15	1	1 (100)	0 (0)	0 (0)
Rectum	V48Gy<=50	3	3 (100)	0 (0)	0 (0)
Rectum	V52Gy<=35	3	3 (100)	0 (0)	0 (0)
Rectum	V56Gy<=25	3	3 (100)	0 (0)	0 (0)
Bladder	V60Gy<=40	16	16 (100)	0 (0)	0 (0)
Bladder	V70Gy<=20	16	15 (94)	0 (0)	1 (6)
Bladder	V65Gy<=20	1	1 (100)	0 (0)	0 (0)
Bladder	V52Gy<=50	3	3 (100)	0 (0)	0 (0)
Bladder	V56Gy<=35	3	3 (100)	0 (0)	0 (0)
Bladder	V60Gy<=25	3	3 (100)	0 (0)	0 (0)
Femoral Heads	V35Gy<=50	1	1 (100)	0 (0)	0 (0)
Femoral Heads	V40Gy<=10	1	1 (100)	0 (0)	0 (0)
Femoral Heads	V45Gy<=2	1	1 (100)	0 (0)	0 (0)
Femoral Heads	V50Gy<=10	19	19 (100)	0 (0)	0 (0)
Femoral Heads	D_{max} <=54	19	19 (100)	0 (0)	0 (0)
Small Bowel	V25Gy<=50	1	1 (100)	0 (0)	0 (0)
Small Bowel	V45Gy<=33	1	1 (100)	0 (0)	0 (0)
Small Bowel	V52Gy<=2	1	1 (100)	0 (0)	0 (0)
Sigmoid	D_{max} <=60	20	20 (100)	0 (0)	0 (0)
PenileBulb	D_{mean} <=54	20	20 (100)	0 (0)	0 (0)

Table 9 Summary for auto-plans meeting, within 5% of or greater than 5% of dosimetric recommendations on manually drawn contour set for four radiation treatment prescriptions: three on prostate and seminal vesicle targets for 78, 72, and 60 Gy and one on the prostate bed and SV-fossa targets for 70 Gy.

Structure	Constraint	No. Cases	Manual Contour, No. (%)		
			<u>Met</u>	<u>Within 5%</u>	<u>Greater than 5%</u>
PTV_7000	V70Gy>=98%	16	16 (100)	0 (0)	0 (0)
PTV_7000	Max<=75.6Gy	16	15 (93.75)	1 (6.25)	0 (0)
PTV_5040	V50.4Gy>=98	16	15 (93.75)	1 (6.25)	0 (0)
PTV_5980	V59.8Gy>=98%	4	3 (75)	1 (25)	0 (0)
PTV_5980	D_{max} <=64.6Gy	4	3 (75)	1 (25)	0 (0)
PTV_4600	V46Gy>=98%	4	3 (75)	1 (25)	0 (0)
Rectum	V65Gy<=15%	16	16 (100)	0 (0)	0 (0)
Rectum	V60Gy<=20%	16	16 (100)	0 (0)	0 (0)

Rectum	V60Gy<=11cc	4	3 (75)	1 (25)	0 (0)
Rectum	V55Gy<=25%	16	16 (100)	0 (0)	0 (0)
Rectum	V54Gy<=15%	4	4 (100)	0 (0)	0 (0)
Rectum	V45Gy<=45%	16	16 (100)	0 (0)	0 (0)
Rectum	V35Gy<=60%	20	20 (100)	0 (0)	0 (0)
Rectum	V25Gy<=80%	20	19 (95)	1 (5)	0 (0)
Bladder	V65Gy<=15%	16	16 (100)	0 (0)	0 (0)
Bladder	V60Gy<=15%	4	4 (100)	0 (0)	0 (0)
Bladder	V55Gy<=25%	16	16 (100)	0 (0)	0 (0)
Bladder	V54Gy<=25%	4	4 (100)	0 (0)	0 (0)
Bladder	V45Gy<=45%	20	17 (85)	2 (10)	1 (5)
Bowel	D_{max} <=54Gy	20	15 (75)	4 (20)	1 (5)
Sigmoid	D_{max} =60Gy	20	20 (100)	0 (0)	0 (0)
PenileBulb	D_{mean} <=54Gy	20	20 (100)	0 (0)	0 (0)
Femoral Heads	D_{max} <=54Gy	20	20 (100)	0 (0)	0 (0)
Femoral Heads	V50Gy<=10%	20	20 (100)	0 (0)	0 (0)
Spinal Cord	D_{max} <=54Gy	20	20 (100)	0 (0)	0 (0)
Cauda Equina	D_{max} <=54Gy	20	20 (100)	0 (0)	0 (0)

Table 10 Summary for auto-plans meeting, within 5% of or greater than 5% of dosimetric recommendations on manually drawn contour set for two radiation treatment prescriptions on prostate and lymph node targets: 70 & 50.4Gy in 35 fractions and 59.8 & 46Gy in 35 fractions.

End-to-End Evaluation

A summary of the quantitative evaluation of clinical dose constraints on auto-plans generated from auto-segmented contours is listed in Table 10 through Table 12. There is considerable agreement between auto-contours and clinical contours for prostate and seminal vesicle targets. For CTV dose constraints, at least 90% of auto-contoured CTVs would have met the same constraint within 5% on the clinical contours. For PTV dose constraints, at least 35% of auto-generated PTVs would have met the same constraint within 5% of the clinical PTVs. For prostate bed and SV-Fossa targets, there is also a considerable agreement between the achievement of dose constraint goals between auto-contours and clinical contours. For CTV dose constraints, all auto-contoured CTVs would have met the same constraint within 5% on the clinical contours. For PTV dose constraints, at least 50% of auto-generated PTVs and clinical PTVs would have met the same constraint within 5%. However, we see lower agreement between auto-contours and clinical contours for prostate and nodal targets. At least 75% of all auto-counteracted CTVs would have met the same constraint within 5% on the clinical

contours. Then, for PTV dose constraints, at least 10% of auto-generated PTVs would have met the same constraint within 5% on the clinical PTVs.

The prostate model achieved dose constraints for normal tissues more readily than the prostate and node model. For intact prostate plans, rectum, bladder, and femoral head dose constraints were achieved for at least 90% of auto-contours and clinical contours. For sigmoid, at least 69% auto contour and clinical contours met the max dose constraint of 60Gy. For postop prostate plans, rectum, bladder, and femoral head dose constraints were achieved for at least 89% of auto-contours and clinical contours. For cases where rectum and bladder high dose constraints were greater than 5%, auto-contours and clinical contours contained high curvature and odd total volume, respectively. For sigmoid, at least 89% of clinical cases have sigmoid contours present. More normal tissue constraints were greater than 5% for prostate and node plans. At least 50% of all auto-contours and clinical contours for the rectum and bladder were achieved within 5% of dose constraints. For sigmoid and bowel bag, at least 75% and 95% of all auto-contours and clinical contours were achieved within 5% of dose constraints, respectively. Both sigmoid and penile bulb clinical contours were not delineated in all postop and prostate plus node test cases.

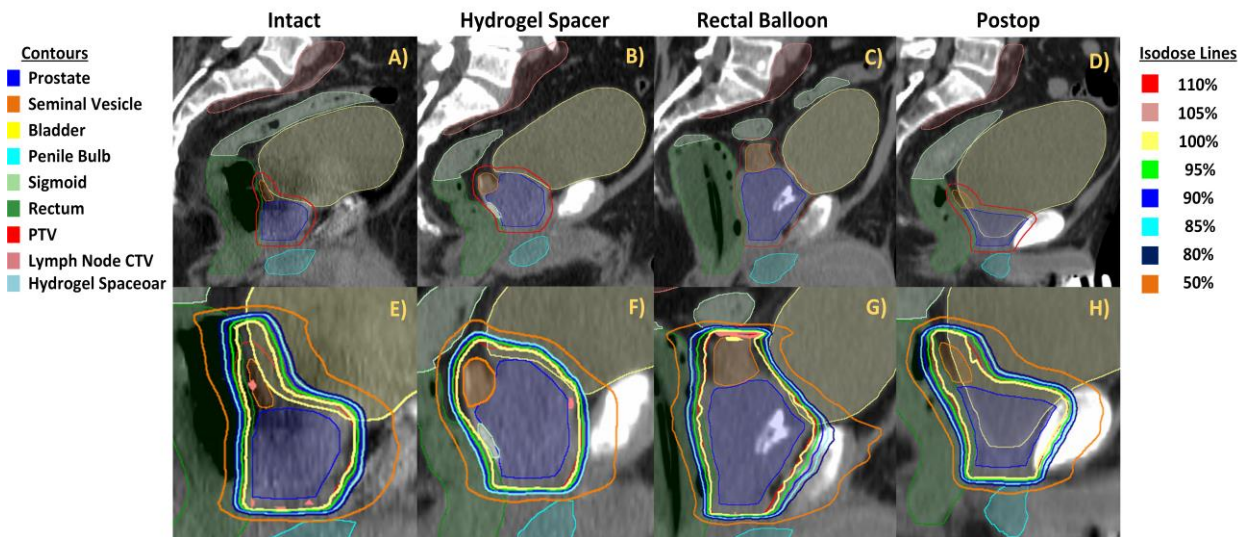


Figure 11 Visualization of automated treatment plans from Prostate only RadidPlan

STRUCTURE	CONSTRAINT	Auto Contour, No. (%)			Clinical Contour, No. (%)		
		<u>Met</u>	<u>Within 5%</u>	<u>Greater than 5%</u>	<u>Met</u>	<u>Within 5%</u>	<u>Greater than 5%</u>
CTV	V78Gy>=100%	23 (88)	3 (12)	0 (0)	9 (35)	15 (58)	2 (8)
CTV	V78Gy>=95%	26 (100)	0 (0)	0 (0)	24 (92)	1 (4)	1 (4)
PTV	V78Gy>=98%	26 (100)	0 (0)	0 (0)	6 (23)	4 (15)	16 (62)
PTV	V78Gy>=95%	26 (100)	0 (0)	0 (0)	7 (27)	7 (27)	12 (46)
PTV	$D_{max} \leq 84.2$ Gy	17 (65)	6 (23)	3 (12)	21 (81)	2 (8)	3 (12)
RECTUM	V30 Gy<=80%	26 (100)	0 (0)	0 (0)	24 (92)	0 (0)	2 (8)
RECTUM	V40 Gy<=60%	26 (100)	0 (0)	0 (0)	24 (92)	0 (0)	2 (8)
RECTUM	V60 Gy<=40%	26 (100)	0 (0)	0 (0)	24 (92)	0 (0)	2 (8)
RECTUM	V70 Gy<=20%	26 (100)	0 (0)	0 (0)	24 (92)	0 (0)	2 (8)
RECTUM	V70 Gy<=15	25 (96)	1 (4)	0 (0)	24 (92)	0 (0)	2 (8)
RECTUM	V76 Gy<=15%	26 (100)	0 (0)	0 (0)	24 (92)	0 (0)	2 (8)
RECTUM	V80 Gy<=5%	26 (100)	0 (0)	0 (0)	24 (92)	0 (0)	2 (8)
BLADDER	V60 Gy<=40%	26 (100)	0 (0)	0 (0)	26 (100)	0 (0)	0 (0)
BLADDER	V70 Gy <=20%	26 (100)	0 (0)	0 (0)	26 (100)	0 (0)	0 (0)
SIGMOID	$D_{max} \leq 60$ Gy	18 (69)	0 (0)	8 (31)	19 (73)	0 (0)	7 (27)
FEMORAL HEADS	V50Gy<=10%	26 (100)	0 (0)	0 (0)	25 (96)	0 (0)	0 (0)
FEMORAL HEADS	$D_{max} \leq 54$ Gy	26 (100)	0 (0)	0 (0)	25 (96)	0 (0)	0 (0)
PENILEBULB	$D_{mean} \leq 54$ Gy	26 (100)	0 (0)	0 (0)	6 (23)	0 (0)	0 (0)

Table 11 Summary for auto-plans meeting, within 5% of or greater than 5% of dosimetric recommendations on auto-contours and clinical contours with radiation treatment prescription on Prostate and seminal vesicle targets of 78Gy in end-to-end testing of treatment pipeline.

STRUCTURE	CONSTRAINT	AUTO CONTOUR, NO. (%)			CLINICAL CONTOUR, NO. (%)		
		<u>Met</u>	<u>Within 5%</u>	<u>Greater than 5%</u>	<u>Met</u>	<u>Within 5%</u>	<u>Greater than 5%</u>
CTV	V70GY>=100%	18 (95)	1 (5)	0 (0)	9 (47)	10 (53)	0 (0)
CTV	V70GY>=95%	19 (100)	0 (0)	0 (0)	19 (100)	0 (0)	0 (0)
PTV	V70GY>=98%	19 (100)	0 (0)	0 (0)	4 (21)	6 (32)	9 (47)
PTV	V70GY>=95%	19 (100)	0 (0)	0 (0)	9 (47)	2 (11)	8 (42)
PTV	$D_{max} \leq 75.6$ GY	7 (37)	12 (63)	0 (0)	7 (37)	12 (63)	0 (0)
RECTUM	V30GY<=80%	19 (100)	0 (0)	0 (0)	19 (100)	0 (0)	0 (0)
RECTUM	V40GY<=60%	19 (100)	0 (0)	0 (0)	19 (100)	0 (0)	0 (0)
RECTUM	V60GY<=40%	18 (95)	1 (5)	0 (0)	19 (100)	0 (0)	0 (0)
RECTUM	V70GY<=15%	17 (89)	0 (0)	2 (11)	18 (95)	0 (0)	1 (5)
BLADDER	V60GY<=40%	19 (100)	0 (0)	0 (0)	19 (100)	0 (0)	0 (0)
BLADDER	V70GY<=20%	17 (89)	0 (0)	2 (11)	17 (89)	1 (5)	1 (5)

SIGMOID	$D_{max} \leq 60\%$	17 (89)	1 (5)	1 (5)	18 (95)	0 (0)	0 (0)
FEMORAL HEADS	$V50GY \leq 10\%$	19 (100)	0 (0)	0 (0)	19 (100)	0 (0)	0 (0)
FEMORAL HEADS	$D_{max} \leq 54$ GY	19 (100)	0 (0)	0 (0)	19 (100)	0 (0)	0 (0)
PENILEBULB	$D_{mean} \leq 54$ GY	18 (95)	1 (5)	0 (0)	2 (11)	0 (0)	1 (5)

Table 12 Summary for auto-plans meeting, within 5% of or greater than 5% of dosimetric recommendations on auto-contours and clinical contours with radiation treatment prescription on Prostate Bed and SV-Fossa targets of 70Gy in end-to-end testing of treatment pipeline.

STRUCTURE	CONSTRAINT	AUTO CONTOUR, NO. (%)			CLINICAL CONTOUR, NO. (%)		
		<u>MET</u>	<u>WITHIN</u> <u>5%</u>	<u>GREATE</u> <u>R THAN</u> <u>5%</u>	<u>MET</u>	<u>WITHIN</u> <u>5%</u>	<u>GREATE</u> <u>R THAN</u> <u>5%</u>
CTV	$V70GY \geq 100\%$	16 (80)	4 (20)	0 (0)	3 (15)	12 (60)	5 (25)
LYMPH NODE CTV	$V50.4GY \geq 100\%$	16 (80)	4 (20)	0 (0)	1 (5)	15 (75)	4 (20)
PTV	$V70GY \geq 98\%$	20 (100)	0 (0)	0 (0)	1 (5)	6 (30)	13 (65)
PTV	$D_{max} \leq 75.6$ GY	7 (35)	13 (65)	0 (0)	10 (50)	10 (50)	0 (0)
LYMPH NODE PTV	$V50.4GY \geq 98\%$	20 (100)	0 (0)	0 (0)	0 (0)	2 (10)	18 (90)
RECTUM	$V65GY \leq 15\%$	6 (30)	4 (20)	10 (50)	13 (65)	1 (5)	6 (30)
RECTUM	$V60GY \leq 20\%$	8 (40)	2 (10)	10 (50)	14 (70)	0 (0)	6 (30)
RECTUM	$V55GY \leq 25\%$	9 (45)	1 (5)	10 (50)	13 (65)	2 (10)	5 (25)
RECTUM	$V45GY \leq 45\%$	15 (75)	0 (0)	5 (25)	11 (55)	3 (15)	6 (30)
RECTUM	$V35GY \leq 60\%$	15 (75)	0 (0)	5 (25)	10 (50)	2 (10)	8 (40)
RECTUM	$V25GY \leq 80\%$	15 (75)	2 (10)	3 (15)	10 (50)	3 (15)	7 (35)
BLADDER	$V65GY \leq 15\%$	8 (40)	2 (10)	10 (50)	10 (50)	0 (0)	10 (50)
BLADDER	$V55GY \leq 25\%$	15 (75)	0 (0)	5 (25)	15 (75)	0 (0)	5 (25)
BLADDER	$V45GY \leq 45\%$	15 (75)	2 (10)	3 (15)	15 (75)	2 (10)	3 (15)
BOWEL	$D_{max} \leq 54$ GY	0 (0)	19 (95)	1 (5)	3 (15)	16 (80)	1 (5)
SIGMOID	$D_{max} = 60$ GY	14 (70)	1 (5)	5 (25)	0 (0)	18 (90)	0 (0)
PENILEBULB	$D_{mean} \leq 54$ GY	17 (85)	1 (5)	2 (10)	2 (10)	0 (0)	2 (10)
FEMORAL HEADS	$D_{max} \leq 54$ GY	20 (100)	0 (0)	0 (0)	20 (100)	0 (0)	0 (0)

FEMORAL HEADS	V50GY<=10%	20 (100)	0 (0)	0 (0)	20 (100)	0 (0)	0 (0)
SPINAL CORD	D_{max} <=54GY	20 (100)	0 (0)	0 (0)	20 (100)	0 (0)	0 (0)
CAUDA EQUINA	D_{max} <=54 GY	20 (100)	0 (0)	0 (0)	20 (100)	0 (0)	0 (0)

Table 13 Summary for auto-plans meeting, within 5% of or greater than 5% of dosimetric recommendations on auto-contours and clinical contours with radiation treatment prescription on prostate and lymph node targets of 70 & 50.4Gy in end-to-end testing of treatment pipeline.

Discussion

Two RapidPlan models were previously developed for a breadth of prostate treatment scenarios and used in end-to-end testing of the proposed treatment pipeline. The first RapidPlan model developed was able to produce VMAT plans for both intact and postoperative prostate with and without the presence of spacers or rectal balloons. The second RapidPlan model was developed to contour prostate cases with Lymph Node involvement again with the presence of hydrogel spacers or rectal balloons. Plans generated from manual contours resulted in greater acceptance from physician reviewers than those generated from auto contours. However, for most end-to-end evaluated cases, the differences in pass rates when compared to clinical contours were not greater than 5% of dose constraints in most cases. At least 50% of all treatment cases created from auto-plans would have passed on the clinical contours for targets and normal tissues. For the review of plans, the choice of the Likert scale was used based on established use in literature for use in automated planning algorithms (Baroudi et al., 2023; Huang et al., 2022).

Reviewers of the auto-generated intact and postop plans commented on the hotspot for both treatment cases. For intact patients, the hotspots remained within the PTVs; however, the location of these hotspots tended to be superior to the prostate within the Seminal Vesicles and close to the rectum and sigmoid. For postop patients, the dose of the overall postoperative CTV was high, resulting in an excess dose to 10% of bladder and rectum patients. Other developed RapidPlan models reported a similar increase in high-dose bladder constraints, although mean doses remained low (Kubo et al., 2017). It was recommended that the mean doses of plans

without nodal involvement be lowered. This was most notable in reviewed postoperative cases, mainly where the bladder descended deep within the resected postoperative prostate cavity.

For prostate and node plans, the rate of meeting dose constraints was not sufficient to obtain physician review. Auto-contours exhibited hotspots around the periphery of the prostate PTV, which resulted in higher doses of the clinical sigmoid. High dose gradients around the unions of the Lymph node PTV and the prostate PTV resulted in higher doses to the bowel, causing both auto contours and clinical contours to pass this constraint but remain within 3 Gy of the constraint. For patients not passing rectum and bladder constraints, high rectum curvatures at the level of the prostate and bladders descending deep into the resected prostate bed are anatomical patterns creating challenging treatment scenarios for automation. Highly curved rectum contours border a larger volume of the resected prostate bed, causing a large area for high-dose gradients to form. Descending bladder contours into the prostate bed results in larger doses to the bladder that are difficult to optimize to give overlap with the target volume. The model for prostate and nodes was developed with a set of 37 patients with a 2:3 ratio of intact and postoperative prostate with node treatment plans. However, the examined auto-contour set was mostly postoperative prostate and node plans; therefore, it is probable that the high curvature and descending bladder anatomies and resultant treatment parameters are not well represented in the model, and DVH optimization is strained to meet constraints for these scenarios. However, based on a review of contours for the postoperative prostate, redress of the excessive size of the prostate bed and SV-fossa must occur first before stress testing of the prostate and node model can be considered.

Conclusion

The study proposed, developed, and tested automated solutions to create VMAT prostate radiotherapy treatment plans. The study demonstrated the ability of RapidPlan models to create acceptable treatment plans for a breadth of prostate treatment scenarios, including intact, postoperative, and lymph node-involved prostate cases, in an end-to-end manner.

Postoperative treatment volumes present a challenge for end-to-end automated treatment approaches to achieve the desired threshold of clinical acceptability. The results of this study demonstrate the ability to meet clinical dose constraints on clinical targets from predicted contours.

CHAPTER 5: DISCUSSION AND CONCLUSION

Project Summary

The main goal of this project was to automate the treatment planning process for prostate cancer radiotherapy. A two-stage treatment pipeline of auto-segmentation and auto-planning was proposed to achieve this goal. The resultant pipeline serves as a minimal interaction system to generate complete VMAT treatment plans from predicted target and normal tissue structures. The segmentation of a breadth of commonly included prostate structures and their corresponding treatment plans were automated and reviewed for clinical acceptability in an end-to-end method.

The chapter on automated contouring presents our solution for the automation of intact and postoperative structures with and without treatment devices and nodal involvement of the disease. Our approach involved using multiple nnU-Net models to generate tissue-specific and volumetric segmentation of target tissues and organs at risk. Target and normal tissue structures were separated into distinctive models to enhance model robustness to unique feature spaces and allow the flexibility of contouring structures that are or are not needed in treatment. Additional post-processing was added to resultant contours to ensure adherence to contouring guidelines and resolve segmentation inaccuracies resulting from independent model predictions. Planning target volumes were generated with input margins depending on the prescribed target structures.

When considering the quantitative results of the proposed model methods to those reported in the literature, our model structures are within the reported overlap and distance metrics range in recent years (see Table 6). While the proposed contouring methods were not the highest achieving in terms of DSC and HD95, it must also be taken into consideration that the models proposed in the literature do not account for treatment scenarios of tissue-specific and volumetric contouring with image artifacts and treatment devices in the same contouring model. Additionally, the contouring datasets are smaller and encompass a shorter history of

clinical contouring practice without detail to large scopes of treatment anatomies or contouring styles across physicians present in simulation CT image data at an institution.

From the review of auto-contours, no contours presented were found to contain more than minor edits. While this demonstrates that all contours currently generated from these proposed models are clinically usable, they are not at the hypothesized threshold of clinical acceptability. However, it was established in this study that the proposed auto-contours were more efficient to edit than contouring from scratch. The benchmark for clinical acceptability with minor edits is within the range of similar studies of prostate cancer contouring in the literature (Cha et al., 2021; Kiljunen et al., 2020). The distinction between stylistic and necessary edits evaluated in this study was important in extracting necessary information about the fitness of contours for clinical implementation. This was most notable in the contour review of postoperative target structures and their corresponding normal tissues. Greater improvement in target structures would be in border delineations to exclude vessels, nerves, and muscles adjacent to these target volumes. For normal tissue structures, the greatest improvement would be in delineating the boundaries between the rectum and sigmoid and providing a more quantifiable definition of accession and transition curvature.

The chapter on automated planning presents our solution for the automated generation of VMAT treatment plans for prostate cancer. Through the use of two RapidPlan models, contours generated for each patient simulation CT were then analyzed to provide an initial DVH estimation from the initial optimization of a plan, which is guided by the DVH estimation. Subsequent optimization iterations for prostate and prostate with node cases reduce plan hotspots and improve target conformality while shifting radiation delivery away from key organs at risk. The resultant plans are then normalized to meet the prescription if they have not already been achieved through the subsequent optimization iterations. Upon quantitative evaluation of manual and end-to-end treatment plans, most treatment plans passed dosimetric constraints. For the majority of constraints not met through the proposed end-to-end process, the plans were within 5% of clinical dose constraints. Furthermore, trends meeting dose constraints on

auto-contours translated to clinical contours in those constraints that did not pass on auto-contours would also not pass on the control group of manually drawn clinical contours. This indicates that the proposed auto-plans generated from auto-contours serve as a plausible representation of reviewed and accepted clinical structures. When considering the 45 automatically generated VMAT plans generated from auto-contours reviewed by physicians, at least 80% of intact and 58% of postop treatment plans scored as requiring no more than minor stylistic edits; this indicates that the plans are useable and able to be optimized to become clinically acceptable after necessary edits are performed.

Study Limitations and Future Directions

The methodology employed in our study exhibits several limitations that warrant consideration. Firstly, although our dataset encompasses a diverse range of treatment cases, our exploration of dosimetric evaluation of auto contours was confined to a singular prescription for intact and postoperative treatments with or without nodal involvement. The choice of prescriptions in this investigation was selected to evaluate the potential to meet dosimetric constraints for hyper-fractionated treatments of high-dose regimens within our institution and those recommended according to accepted treatment guidelines (“ NCCN guidelines: prostate cancer (version 3.2024)., ”). This narrow scope restricts the generalizability of our findings to broader treatment contexts in which hypo-fractionated treatments or treatments of multiple dose levels are administered (Kaderka et al., 2019; Langrand-Escure et al., 2018; Qureshy et al., 2023). While changes in the current knowledge base of prior treatments in the RapidPlan models used would need to be adjusted for hypofractionated treatments, evaluation of multiple dose levels is within the scope of current models to evaluate the pass rates of clinical dose constraints.

While contour review was performed as a direct categorical score of quality (i.e., score contours and then score plan), contour performance could be evaluated in follow-up inquiries by asking physicians what adjustments they would make to auto-segmented contours upon

review of the treatment plan. As the questioning and feedback of contour review were performed with a direct score of each individual contour for acceptability, feedback on contour quality was generated in the absence of viewing the plan. Quantitative metrics require a qualitative review to elucidate the intricate numerical features in the context of correct anatomy and adherence to clinical practice and guidelines (Reinke et al., 2023). Therefore, contour usability would be more appreciated in the context of structure delineation when a course of radiation delivery is presented. Methods to include physician edits in auto-segmentation approaches have been proposed through graph neural network-based models on MR images (Tian et al., 2020).

With regard to medical imaging data, the focus was exclusively on CT data. The exclusion of other imaging modalities leads to the underuse of imaging technologies used in clinical settings to overcome limitations in soft tissue contrast to delineate structures. MR imaging, with enhanced soft-tissue contrast coupled with CT imaging, would overcome difficulties in addressing low contrast boundaries and variations in noise/appearance patterns in basal and apical regions of the prostate (Tian et al., 2020). MR-based deep learning approaches are a continued area of research for medical imaging segmentation, including the use of CT and MR fusion images (Almeida and Tavares, 2020). Moreover, our investigation was constrained by the utilization of a single set of guidelines for each contour, neglecting the potential variability introduced by employing alternative guideline frameworks. Additionally, the inclusion criteria for contours were restricted to those conforming to specific guidelines, disregarding potential clinical factors that may influence deviations from these guidelines (Li et al., 2021). This narrow selection criterion may limit the comprehensiveness of our analysis and the extrapolation of our findings to clinical scenarios at other institutions.

Considering these limitations, several avenues for future research emerge. One prospective direction involves revisiting the planning approach while incorporating modified contours, thereby assessing the impact of such adjustments on treatment outcomes. This is to act not only as an end-to-end evaluation of our pipeline performance but also to assess the

extent to which corrected plans match manual plan performance and clinical acceptance. Furthermore, the location and effort in edits can be quantified and tracked through metrics such as added path length, which have been used to study the effect of edits on contour and planning time (Cha et al., 2021; Vaassen et al., 2020). Additionally, conducting quality assurance checks on the auto contours by comparing them with alternative auto-contouring methodologies could provide valuable insights into the robustness and reliability of the current contouring techniques. Studies using multiple models to evaluate outliers or abnormalities in cervical and head and neck cancers for both contour and plan quality (Gronberg et al., 2022; Rhee et al., 2019). Such endeavors promise to advance the understanding and efficacy of contouring practices in clinical settings.

Conclusion

The work presented in this thesis demonstrates the potential for end-to-end treatment planning for prostate cancer through automated segmentation and automated planning of the prostate radiotherapy workflow process.

BIBLIOGRAPHY

- Ahn, S.H., Kim, E., Kim, C., Cheon, W., Kim, M., Lee, S.B., Lim, Y.K., Kim, H., Shin, D., Kim, D.Y., Jeong, J.H., 2021. Deep learning method for prediction of patient-specific dose distribution in breast cancer. *Radiat. Oncol. Lond. Engl.* 16, 154.
<https://doi.org/10.1186/s13014-021-01864-9>
- Ahn, S.H., Yeo, A.U., Kim, K.H., Kim, C., Goh, Y., Cho, S., Lee, S.B., Lim, Y.K., Kim, H., Shin, D., Kim, T., Kim, T.H., Youn, S.H., Oh, E.S., Jeong, J.H., 2019. Comparative clinical evaluation of atlas and deep-learning-based auto-segmentation of organ structures in liver cancer. *Radiat. Oncol.* 14, 213. <https://doi.org/10.1186/s13014-019-1392-z>
- Almeida, G., Tavares, J.M.R.S., 2020. Deep Learning in Radiation Oncology Treatment Planning for Prostate Cancer: A Systematic Review. *J. Med. Syst.* 44, 179.
<https://doi.org/10.1007/s10916-020-01641-3>
- Ayuthaya, I.I.N., Sanghangthum, T., Oonsiri, P., Oonsiri, S., Keawsamur, M., Ruangchan, S., Vannavijit, C., Kanphet, J., Kingkaew, S., Vimolnoch, M., Tawonwong, T., Plangpleng, N., 2023. Multi-planner validation of RapidPlan knowledge-based model for volumetric modulated arc therapy in prostate cancer. *J. Appl. Clin. Med. Phys.* 25, e14223.
<https://doi.org/10.1002/acm2.14223>
- Balagopal, A., Kazemifar, S., Nguyen, D., Lin, M.-H., Hannan, R., Owringi, A., Jiang, S., 2018. Fully automated organ segmentation in male pelvic CT images. *Phys. Med. Biol.* 63, 245015. <https://doi.org/10.1088/1361-6560/aaf11c>
- Balagopal, A., Nguyen, D., Morgan, H., Weng, Y., Dohopolski, M., Lin, M.-H., Barkousaraie, A.S., Gonzalez, Y., Garant, A., Desai, N., Hannan, R., Jiang, S., 2021. A deep learning-based framework for segmenting invisible clinical target volumes with estimated uncertainties for post-operative prostate cancer radiotherapy. *Med. Image Anal.* 72, 102101. <https://doi.org/10.1016/j.media.2021.102101>
- Baroudi, H., Brock, K.K., Cao, W., Chen, X., Chung, C., Court, L.E., El Basha, M.D., Farhat, M., Gay, S., Gronberg, M.P., Gupta, A.C., Hernandez, S., Huang, K., Jaffray, D.A., Lim, R.,

- Marquez, B., Nealon, K., Netherton, T.J., Nguyen, C.M., Reber, B., Rhee, D.J., Salazar, R.M., Shanker, M.D., Sjogreen, C., Woodland, M., Yang, J., Yu, C., Zhao, Y., 2023. Automated Contouring and Planning in Radiation Therapy: What Is 'Clinically Acceptable'? *Diagnostics* 13, 667. <https://doi.org/10.3390/diagnostics13040667>
- Beesley, L.J., Morgan, T.M., Spratt, D.E., Singhal, U., Feng, F.Y., Furgal, A.C., Jackson, W.C., Daignault, S., Taylor, J.M.G., 2019. Individual and Population Comparisons of Surgery and Radiotherapy Outcomes in Prostate Cancer Using Bayesian Multistate Models. *JAMA Netw. Open* 2, e187765. <https://doi.org/10.1001/jamanetworkopen.2018.7765>
- Cahlon, O., Hunt, M., Zelefsky, M.J., 2008. Intensity-Modulated Radiation Therapy: Supportive Data for Prostate Cancer. *Semin. Radiat. Oncol.*, Advances in the Management of Prostate Cancer 18, 48–57. <https://doi.org/10.1016/j.semradonc.2007.09.007>
- Cha, E., Elguindi, S., Onochie, I., Gorovets, D., Deasy, J.O., Zelefsky, M., Gillespie, E.F., 2021. Clinical implementation of deep learning contour autosegmentation for prostate radiotherapy. *Radiother. Oncol. J. Eur. Soc. Ther. Radiol. Oncol.* 159, 1–7. <https://doi.org/10.1016/j.radonc.2021.02.040>
- Chen, R.C., Basak, R., Meyer, A.-M., Kuo, T.-M., Carpenter, W.R., Agans, R.P., Broughman, J.R., Reeve, B.B., Nielsen, M.E., Usinger, D.S., Spearman, K.C., Walden, S., Kaleel, D., Anderson, M., Stürmer, T., Godley, P.A., 2017. Association Between Choice of Radical Prostatectomy, External Beam Radiotherapy, Brachytherapy, or Active Surveillance and Patient-Reported Quality of Life Among Men With Localized Prostate Cancer. *JAMA* 317, 1141–1150. <https://doi.org/10.1001/jama.2017.1652>
- Comelli, A., Dahiya, N., Stefano, A., Vernuccio, F., Portoghese, M., Cutaia, G., Bruno, A., Salvaggio, G., Yezzi, A., 2021. Deep Learning-Based Methods for Prostate Segmentation in Magnetic Resonance Imaging. *Appl. Sci. Basel Switz.* 11, 782. <https://doi.org/10.3390/app11020782>

- Conroy, L., Khalifa, A., Berlin, A., McIntosh, C., Purdie, T.G., 2021. Performance stability evaluation of atlas-based machine learning radiation therapy treatment planning in prostate cancer. *Phys. Med. Biol.* 66, 134001. <https://doi.org/10.1088/1361-6560/abfff0>
- Dal Pra, A., Dirix, P., Khoo, V., Carrie, C., Cozzarini, C., Fonteyne, V., Ghadjar, P., Gomez-Iturriaga, A., Panebianco, V., Zapatero, A., Bossi, A., Wiegel, T., 2023. ESTRO ACROP guideline on prostate bed delineation for postoperative radiotherapy in prostate cancer. *Clin. Transl. Radiat. Oncol.* 41, 100638. <https://doi.org/10.1016/j.ctro.2023.100638>
- Duan, J., Bernard, M., Downes, L., Willows, B., Feng, X., Mourad, W.F., St Clair, W., Chen, Q., 2022. Evaluating the clinical acceptability of deep learning contours of prostate and organs-at-risk in an automated prostate treatment planning process. *Med. Phys.* 49, 2570–2581. <https://doi.org/10.1002/mp.15525>
- Elisabeth Olsson, C., Suresh, R., Niemelä, J., Akram, S.U., Valdman, A., 2022. Autosegmentation based on different-sized training datasets of consistently-curated volumes and impact on rectal contours in prostate cancer radiation therapy. *Phys. Imaging Radiat. Oncol.* 22, 67–72. <https://doi.org/10.1016/j.phro.2022.04.007>
- Fogliata, A., Cozzi, L., Reggiori, G., Stravato, A., Lobefalo, F., Franzese, C., Franceschini, D., Tomatis, S., Scorsetti, M., 2019. RapidPlan knowledge based planning: iterative learning process and model ability to steer planning strategies. *Radiat. Oncol.* 14, 187. <https://doi.org/10.1186/s13014-019-1403-0>
- Fogliata, A., Parabolicoli, S., Paganini, L., Reggiori, G., Lobefalo, F., Cozzi, L., Franzese, C., Franceschini, D., Spoto, R., Scorsetti, M., 2022. Knowledge-based DVH estimation and optimization for breast VMAT plans with and without avoidance sectors. *Radiat. Oncol.* 17, 200. <https://doi.org/10.1186/s13014-022-02172-6>
- Gay, H.A., Barthold, H.J., O'Meara, E., Bosch, W.R., El Naqa, I., Al-Lozi, R., Rosenthal, S.A., Lawton, C., Lee, W.R., Sandler, H., Zietman, A., Myerson, R., Dawson, L.A., Willett, C., Kachnic, L.A., Jhingran, A., Portelance, L., Ryu, J., Small, W., Gaffney, D., Viswanathan, A.N., Michalski, J.M., 2012. Pelvic Normal Tissue Contouring Guidelines for Radiation

- Therapy: A Radiation Therapy Oncology Group Consensus Panel Atlas. *Int. J. Radiat. Oncol. Biol. Phys.* 83, e353–e362. <https://doi.org/10.1016/j.ijrobp.2012.01.023>
- Ge, Y., Wu, Q.J., 2019. Knowledge-based planning for intensity-modulated radiation therapy: A review of data-driven approaches. *Med. Phys.* 46, 2760–2775. <https://doi.org/10.1002/mp.13526>
- Good, D., Lo, J., Lee, W.R., Wu, Q.J., Yin, F.-F., Das, S.K., 2013. A Knowledge-Based Approach to Improving and Homogenizing Intensity Modulated Radiation Therapy Planning Quality Among Treatment Centers: An Example Application to Prostate Cancer Planning. *Int. J. Radiat. Oncol.* 87, 176–181. <https://doi.org/10.1016/j.ijrobp.2013.03.015>
- Gooding, M.J., Smith, A.J., Tariq, M., Aljabar, P., Peressutti, D., 2018. Comparative evaluation of autocontouring in clinical practice: A practical method using the Turing test. *Med. Phys.* 45, 5105–5115. <https://doi.org/10.1002/mp.13200>
- Gray, P.J., Lin, C.C., Cooperberg, M.R., Jemal, A., Efstathiou, J.A., 2017. Temporal Trends and the Impact of Race, Insurance, and Socioeconomic Status in the Management of Localized Prostate Cancer. *Eur. Urol.* 71, 729–737. <https://doi.org/10.1016/j.eururo.2016.08.047>
- Gronberg, M.P., Beadle, B.M., Garden, A.S., Skinner, H., Gay, S., Netherton, T., Cao, W., Cardenas, C.E., Chung, C., Fuentes, D., Fuller, C.D., Howell, R.M., Jhingran, A., Lim, T.Y., Marquez, B., Mumme, R., Olanrewaju, A.M., Peterson, C.B., Vazquez, I., Whitaker, T.J., Wooten, Z., Yang, M., Court, L.E., 2022. Deep Learning-Based Dose Prediction for Automated, Individualized Quality Assurance of Head and Neck Radiotherapy Plans. <https://doi.org/10.48550/arXiv.2209.14277>
- Hall, W.A., Paulson, E., Davis, B.J., Spratt, D.E., Morgan, T.M., Dearnaley, D., Tree, A.C., Efstathiou, J.A., Harisinghani, M., Jani, A.B., Buyyounouski, M.K., Pisansky, T.M., Tran, P.T., Karnes, R.J., Chen, R.C., Cury, F.L., Michalski, J.M., Rosenthal, S.A., Koontz, B.F., Wong, A.C., Nguyen, P.L., Hope, T.A., Feng, F., Sandler, H.M., Lawton, C.A.F., 2021. NRG Oncology Updated International Consensus Atlas on Pelvic Lymph Node Volumes for Intact

and Postoperative Prostate Cancer. *Int. J. Radiat. Oncol.* 109, 174–185.

<https://doi.org/10.1016/j.ijrobp.2020.08.034>

Hamdy, F.C., Donovan, J.L., Lane, J.A., Mason, M., Metcalfe, C., Holding, P., Davis, M., Peters, T.J., Turner, E.L., Martin, R.M., Oxley, J., Robinson, M., Staffurth, J., Walsh, E., Bollina, P., Catto, J., Doble, A., Doherty, A., Gillatt, D., Kockelbergh, R., Kynaston, H., Paul, A., Powell, P., Prescott, S., Rosario, D.J., Rowe, E., Neal, D.E., 2016. 10-Year Outcomes after Monitoring, Surgery, or Radiotherapy for Localized Prostate Cancer. *N. Engl. J. Med.* 375, 1415–1424. <https://doi.org/10.1056/NEJMoa1606220>

Huang, K., Das, P., Olanrewaju, A.M., Cardenas, C., Fuentes, D., Zhang, L., Hancock, D., Simonds, H., Rhee, D.J., Beddar, S., Briere, T.M., Court, L., 2022. Automation of radiation treatment planning for rectal cancer. *J. Appl. Clin. Med. Phys.* 23, e13712. <https://doi.org/10.1002/acm2.13712>

Hwee, J., Louie, A.V., Gaede, S., Bauman, G., D'Souza, D., Sexton, T., Lock, M., Ahmad, B., Rodrigues, G., 2011. Technology assessment of automated atlas based segmentation in prostate bed contouring. *Radiat. Oncol. Lond. Engl.* 6, 110. <https://doi.org/10.1186/1748-717X-6-110>

Isensee, F., Jaeger, P.F., Kohl, S.A.A., Petersen, J., Maier-Hein, K.H., 2021. nnU-Net: a self-configuring method for deep learning-based biomedical image segmentation. *Nat. Methods* 18, 203–211. <https://doi.org/10.1038/s41592-020-01008-z>

Kaderka, R., Hild, S.J., Bry, V.N., Cornell, M., Ray, X.J., Murphy, J.D., Atwood, T.F., Moore, K.L., 2021. Wide-Scale Clinical Implementation of Knowledge-Based Planning: An Investigation of Workforce Efficiency, Need for Post-automation Refinement, and Data-Driven Model Maintenance. *Int. J. Radiat. Oncol.* 111, 705–715. <https://doi.org/10.1016/j.ijrobp.2021.06.028>

Kaderka, R., Mundt, R.C., Li, N., Ziemer, B., Bry, V.N., Cornell, M., Moore, K.L., 2019. Automated Closed- and Open-Loop Validation of Knowledge-Based Planning Routines

Across Multiple Disease Sites. *Pract. Radiat. Oncol.* 9, 257–265.

<https://doi.org/10.1016/j.prro.2019.02.010>

Kazemifar, S., Balagopal, A., Nguyen, D., McGuire, S., Hannan, R., Jiang, S., Owrangi, A., 2018. Segmentation of the prostate and organs at risk in male pelvic CT images using deep learning. *Biomed. Phys. Eng. Express* 4, 055003. <https://doi.org/10.1088/2057-1976/aad100>

Kiljunen, T., Akram, S., Niemelä, J., Löyttyniemi, E., Seppälä, J., Heikkilä, J., Vuolukka, K., Kääriäinen, O.-S., Heikkilä, V.-P., Lehtiö, K., Nikkinen, J., Gershkevitsh, E., Borkvel, A., Adamson, M., Zolotuhhin, D., Kolk, K., Pang, E.P.P., Tuan, J.K.L., Master, Z., Chua, M.L.K., Joensuu, T., Kononen, J., Myllykangas, M., Riener, M., Mokka, M., Keyriläinen, J., 2020. A Deep Learning-Based Automated CT Segmentation of Prostate Cancer Anatomy for Radiation Therapy Planning-A Retrospective Multicenter Study. *Diagnostics* 10, 959. <https://doi.org/10.3390/diagnostics10110959>

Kisling, K., Zhang, L., Simonds, H., Fakie, N., Yang, J., McCarroll, R., Balter, P., Burger, H., Bogler, O., Howell, R., Schmeler, K., Mejia, M., Beadle, B.M., Jhingran, A., Court, L., 2019. Fully Automatic Treatment Planning for External-Beam Radiation Therapy of Locally Advanced Cervical Cancer: A Tool for Low-Resource Clinics. *J. Glob. Oncol.* 1–9. <https://doi.org/10.1200/JGO.18.00107>

Kubo, K., Monzen, H., Ishii, K., Tamura, M., Kawamorita, R., Sumida, I., Mizuno, H., Nishimura, Y., 2017. Dosimetric comparison of RapidPlan and manually optimized plans in volumetric modulated arc therapy for prostate cancer. *Phys. Medica PM Int. J. Devoted Appl. Phys. Med. Biol. Off. J. Ital. Assoc. Biomed. Phys. AIFB* 44, 199–204. <https://doi.org/10.1016/j.ejmp.2017.06.026>

Kubo, K., Monzen, H., Ishii, K., Tamura, M., Nakasaka, Y., Kusawake, M., Kishimoto, S., Nakahara, R., Matsuda, S., Nakajima, T., Kawamorita, R., 2019. Inter-planner variation in treatment-plan quality of plans created with a knowledge-based treatment planning system. *Phys. Med.* 67, 132–140. <https://doi.org/10.1016/j.ejmp.2019.10.032>

- Langrand-Escure, J., de Crevoisier, R., Llagostera, C., Créhange, G., Delaroche, G., Lafond, C., Bonin, C., Bideault, F., Sargos, P., Belhomme, S., Pasquier, D., Latorzeff, I., Supiot, S., Hennequin, C., 2018. Dose constraints for moderate hypofractionated radiotherapy for prostate cancer: The French genito-urinary group (GETUG) recommendations. *Cancer/Radiothérapie* 22, 193–198. <https://doi.org/10.1016/j.canrad.2017.11.004>
- Li, G., Li, Y., Wang, J., Gao, X., Zhong, Q., He, L., Li, C., Liu, M., Liu, Y., Ma, M., Wang, H., Wang, X., Zhu, H., 2021. Guidelines for radiotherapy of prostate cancer (2020 edition). *Precis. Radiat. Oncol.* 5, 160–182. <https://doi.org/10.1002/pro6.1129>
- Liu, Z., Liu, X., Guan, H., Zhen, H., Sun, Y., Chen, Q., Chen, Y., Wang, S., Qiu, J., 2020. Development and validation of a deep learning algorithm for auto-delineation of clinical target volume and organs at risk in cervical cancer radiotherapy. *Radiother. Oncol., Physics Special Issue: ESTRO Physics Research Workshops on Science in Development* 153, 172–179. <https://doi.org/10.1016/j.radonc.2020.09.060>
- Marks, L.B., Yorke, E.D., Jackson, A., Ten Haken, R.K., Constine, L.S., Eisbruch, A., Bentzen, S.M., Nam, J., Deasy, J.O., 2010. Use of Normal Tissue Complication Probability Models in the Clinic. *Int. J. Radiat. Oncol., Quantitative Analyses of Normal Tissue Effects in the Clinic* 76, S10–S19. <https://doi.org/10.1016/j.ijrobp.2009.07.1754>
- Martínez, F., Romero, E., Dréan, G., Simon, A., Haigron, P., De Crevoisier, R., Acosta, O., 2014. Segmentation of pelvic structures for planning CT using a geometrical shape model tuned by a multi-scale edge detector. *Phys. Med. Biol.* 59, 1471–1484. <https://doi.org/10.1088/0031-9155/59/6/1471>
- Michalski, J.M., Lawton, C., El Naqa, I., Ritter, M., O'Meara, E., Seider, M.J., Lee, W.R., Rosenthal, S.A., Pisansky, T., Catton, C., Valicenti, R.K., Zietman, A.L., Bosch, W.R., Sandler, H., Buyyounouski, M.K., Ménard, C., 2010. Development of RTOG Consensus Guidelines for the Definition of the Clinical Target Volume for Postoperative Conformal Radiation Therapy for Prostate Cancer. *Int. J. Radiat. Oncol.* 76, 361–368. <https://doi.org/10.1016/j.ijrobp.2009.02.006>

- Moore, K.L., Brame, R.S., Low, D.A., Mutic, S., 2011. Experience-Based Quality Control of Clinical Intensity-Modulated Radiotherapy Planning. *Int. J. Radiat. Oncol.* 81, 545–551. <https://doi.org/10.1016/j.ijrobp.2010.11.030>
- Moore, K.L., Schmidt, R., Moiseenko, V., Olsen, L.A., Tan, J., Xiao, Y., Galvin, J., Pugh, S., Seider, M.J., Dicker, A.P., Bosch, W., Michalski, J., Mutic, S., 2015. Quantifying Unnecessary Normal Tissue Complication Risks due to Suboptimal Planning: A Secondary Study of RTOG 0126. *Int. J. Radiat. Oncol.* 92, 228–235. <https://doi.org/10.1016/j.ijrobp.2015.01.046>
- National Comprehensive Cancer Network. NCCN guidelines: prostate cancer (version 3.2024). [WWW Document], n.d. . NCCN. URL <https://www.nccn.org/guidelines/guidelines-detail> (accessed 3.25.24).
- Oktay, O., Nanavati, J., Schwaighofer, A., Carter, D., Bristow, M., Tanno, R., Jena, R., Barnett, G., Noble, D., Rimmer, Y., Glocker, B., O'Hara, K., Bishop, C., Alvarez-Valle, J., Nori, A., 2020. Evaluation of Deep Learning to Augment Image-Guided Radiotherapy for Head and Neck and Prostate Cancers. *JAMA Netw. Open* 3, e2027426. <https://doi.org/10.1001/jamanetworkopen.2020.27426>
- Orton, C.G., Bortfeld, T.R., Niemierko, A., Unkelbach, J., 2008. The role of medical physicists and the AAPM in the development of treatment planning and optimization. *Med. Phys.* 35, 4911–4923. <https://doi.org/10.1118/1.2990777>
- Pan, H., Feng, Y., Chen, Q., Meyer, C., Feng, X., 2019. Prostate Segmentation From 3D Mri Using A Two-Stage Model and Variable-Input Based Uncertainty Measure, in: 2019 IEEE 16th International Symposium on Biomedical Imaging (ISBI 2019). Presented at the 2019 IEEE 16th International Symposium on Biomedical Imaging (ISBI 2019), pp. 468–471. <https://doi.org/10.1109/ISBI.2019.8759300>
- Qureshy, S.A., Diven, M.A., Ma, X., Marciscano, A.E., Hu, J.C., McClure, T.D., Barbieri, C., Nagar, H., 2023. Differential Use of Radiotherapy Fractionation Regimens in Prostate

Cancer. JAMA Netw. Open 6, e2337165.

<https://doi.org/10.1001/jamanetworkopen.2023.37165>

Reddy, N.M.S., Nori, D., Chang, H., Lange, C.S., Ravi, A., 2010. Prostate and seminal vesicle volume based consideration of prostate cancer patients for treatment with 3D-conformal or intensity-modulated radiation therapy). *Med. Phys.* 37, 3791–3801.

<https://doi.org/10.1118/1.3451125>

Reid, L., 2019. A multiple comparison study that test the validity of Varian's RapidPlan for prostate cancer cases based on models built from outside institution. *Culminating Exp. Proj.*

Reinke, A., Tizabi, M.D., Sudre, C.H., Eisenmann, M., Rädtsch, T., Baumgartner, M., Acion, L., Antonelli, M., Arbel, T., Bakas, S., Bankhead, P., Benis, A., Blaschko, M., Buettner, F., Cardoso, M.J., Chen, J., Cheplygina, V., Christodoulou, E., Cimini, B., Collins, G.S., Engelhardt, S., Farahani, K., Ferrer, L., Galdran, A., van Ginneken, B., Glocker, B., Godau, P., Haase, R., Hamprecht, F., Hashimoto, D.A., Heckmann-Nötzel, D., Hirsch, P., Hoffman, M.M., Huisman, M., Isensee, F., Jannin, P., Kahn, C.E., Kainmueller, D., Kainz, B., Karargyris, A., Karthikesalingam, A., Kavur, A.E., Kenngott, H., Kleesiek, J., Kleppe, A., Kohler, S., Kofler, F., Kopp-Schneider, A., Kooi, T., Kozubek, M., Kreshuk, A., Kurc, T., Landman, B.A., Litjens, G., Madani, A., Maier-Hein, K., Martel, A.L., Mattson, P., Meijering, E., Menze, B., Moher, D., Moons, K.G.M., Müller, H., Nichyporuk, B., Nickel, F., Noyan, M.A., Petersen, J., Polat, G., Rafelski, S.M., Rajpoot, N., Reyes, M., Rieke, N., Riegler, M., Rivaz, H., Saez-Rodriguez, J., Sánchez, C.I., Schroeter, J., Saha, A., Selver, M.A., Sharan, L., Shetty, S., van Smeden, M., Stieltjes, B., Summers, R.M., Taha, A.A., Tiulpin, A., Tsaftaris, S.A., Van Calster, B., Varoquaux, G., Wiesenfarth, M., Yaniv, Z.R., Jäger, P., Maier-Hein, L., 2023. Common Limitations of Image Processing Metrics: A Picture Story.

<https://doi.org/10.48550/arXiv.2104.05642>

Rhee, D.J., Akinfenwa, C.P.A., Rigaud, B., Jhingran, A., Cardenas, C.E., Zhang, L., Prajapati, S., Kry, S.F., Brock, K.K., Beadle, B.M., Shaw, W., O'Reilly, F., Parkes, J., Burger, H.,

- Fakie, N., Trauernicht, C., Simonds, H., Court, L.E., 2022. Automatic contouring QA method using a deep learning–based autocontouring system. *J. Appl. Clin. Med. Phys.* 23, e13647. <https://doi.org/10.1002/acm2.13647>
- Rhee, D.J., Cardenas, C.E., Elhalawani, H., McCarroll, R., Zhang, L., Yang, J., Garden, A.S., Peterson, C.B., Beadle, B.M., Court, L.E., 2019. Automatic detection of contouring errors using convolutional neural networks. *Med. Phys.* 46, 5086–5097. <https://doi.org/10.1002/mp.13814>
- Rhee, D.J., Jhingran, A., Kisling, K., Cardenas, C., Simonds, H., Court, L., 2020. Automated Radiation Treatment Planning for Cervical Cancer. *Semin. Radiat. Oncol., Cervical Cancer* 30, 340–347. <https://doi.org/10.1016/j.semradonc.2020.05.006>
- Rigaud, B., Anderson, B.M., Yu, Z.H., Gobeli, M., Cazoulat, G., Söderberg, J., Samuelsson, E., Lidberg, D., Ward, C., Taku, N., Cardenas, C., Rhee, D.J., Venkatesan, A.M., Peterson, C.B., Court, L., Svensson, S., Löfman, F., Klopp, A.H., Brock, K.K., 2021. Automatic Segmentation Using Deep Learning to Enable Online Dose Optimization During Adaptive Radiation Therapy of Cervical Cancer. *Int. J. Radiat. Oncol.* 109, 1096–1110. <https://doi.org/10.1016/j.ijrobp.2020.10.038>
- Salazar, R.M., Duryea, J.D., Leone, A.O., Nair, S.S., Mumme, R.P., De, B., Corrigan, K.L., Rooney, M.K., Das, P., Holliday, E.B., Court, L.E., Niedzielski, J.S., 2024. Random Forest Modeling of Acute Toxicity in Anal Cancer: Effects of Peritoneal Cavity Contouring Approaches on Model Performance. *Int. J. Radiat. Oncol.* 118, 554–564. <https://doi.org/10.1016/j.ijrobp.2023.08.042>
- Siegel, R.L., Miller, K.D., Wagle, N.S., Jemal, A., 2023. Cancer statistics, 2023. *CA. Cancer J. Clin.* 73, 17–48. <https://doi.org/10.3322/caac.21763>
- Sung, H., Ferlay, J., Siegel, R.L., Laversanne, M., Soerjomataram, I., Jemal, A., Bray, F., 2021. Global Cancer Statistics 2020: GLOBOCAN Estimates of Incidence and Mortality Worldwide for 36 Cancers in 185 Countries. *CA. Cancer J. Clin.* 71, 209–249. <https://doi.org/10.3322/caac.21660>

- Teoh, M., Clark, C.H., Wood, K., Whitaker, S., Nisbet, A., 2011. Volumetric modulated arc therapy: a review of current literature and clinical use in practice. *Br. J. Radiol.* 84, 967–996. <https://doi.org/10.1259/bjr/22373346>
- Tian, Z., Li, X., Zheng, Y., Chen, Z., Shi, Z., Liu, L., Fei, B., 2020. Graph-convolutional-network-based interactive prostate segmentation in MR images. *Med. Phys.* 47, 4164–4176. <https://doi.org/10.1002/mp.14327>
- Vaassen, F., Hazelaar, C., Vaniqui, A., Gooding, M., van der Heyden, B., Canters, R., van Elmpt, W., 2020. Evaluation of measures for assessing time-saving of automatic organ-at-risk segmentation in radiotherapy. *Phys. Imaging Radiat. Oncol.* 13, 1–6. <https://doi.org/10.1016/j.phro.2019.12.001>
- van Gysen, K., O'Toole, J., Le, A., Wu, K., Schuler, T., Porter, B., Kipritidis, J., Atyeo, J., Brown, C., Eade, T., 2020. Rolling out RapidPlan: What we've learnt. *J. Med. Radiat. Sci.* 67, 310–317. <https://doi.org/10.1002/jmrs.420>
- Wang, Y., Boyd, G., Zieminski, S., Kamran, S.C., Zietman, A.L., Miyamoto, D.T., Kirk, M.C., Efstathiou, J.A., 2023. A pair of deep learning auto-contouring models for prostate cancer patients injected with a radio-transparent versus radiopaque hydrogel spacer. *Med. Phys.* 50, 3324–3337. <https://doi.org/10.1002/mp.16375>
- Wu, B., Ricchetti, F., Sanguineti, G., Kazhdan, M., Simari, P., Chuang, M., Taylor, R., Jacques, R., McNutt, T., 2009. Patient geometry-driven information retrieval for IMRT treatment plan quality control. *Med. Phys.* 36, 5497–5505. <https://doi.org/10.1118/1.3253464>
- Yu, C., Anakwenze, C.P., Zhao, Y., Martin, R.M., Ludmir, E.B., S. Niedzielski, J., Qureshi, A., Das, P., Holliday, E.B., Raldow, A.C., Nguyen, C.M., Mumme, R.P., Netherton, T.J., Rhee, D.J., Gay, S.S., Yang, J., Court, L.E., Cardenas, C.E., 2022. Multi-organ segmentation of abdominal structures from non-contrast and contrast enhanced CT images. *Sci. Rep.* 12, 19093. <https://doi.org/10.1038/s41598-022-21206-3>

- Yuan, L., Ge, Y., Lee, W.R., Yin, F.F., Kirkpatrick, J.P., Wu, Q.J., 2012. Quantitative analysis of the factors which affect the interpatient organ-at-risk dose sparing variation in IMRT plans. *Med. Phys.* 39, 6868–6878. <https://doi.org/10.1118/1.4757927>
- Zabel, W.J., Conway, J.L., Gladwish, A., Skliarenko, J., Didiodato, G., Goorts-Matthews, L., Michalak, A., Reistetter, S., King, J., Nakonechny, K., Malkoske, K., Tran, M.N., McVicar, N., 2021. Clinical Evaluation of Deep Learning and Atlas-Based Auto-Contouring of Bladder and Rectum for Prostate Radiation Therapy. *Pract. Radiat. Oncol.* 11, e80–e89. <https://doi.org/10.1016/j.prro.2020.05.013>
- Zarepisheh, M., Long, T., Li, N., Tian, Z., Romeijn, H.E., Jia, X., Jiang, S.B., 2014. A DVH-guided IMRT optimization algorithm for automatic treatment planning and adaptive radiotherapy replanning. *Med. Phys.* 41, 061711. <https://doi.org/10.1118/1.4875700>
- Zhou, Y., Launay, L., Bert, J., de Crevoisier, R., Acosta, O., 2019. Optimized Multi-Atlas Prostate Segmentation From 3D CT Images, in: 2019 IEEE 16th International Symposium on Biomedical Imaging (ISBI 2019). Presented at the 2019 IEEE 16th International Symposium on Biomedical Imaging (ISBI 2019), pp. 32–35. <https://doi.org/10.1109/ISBI.2019.8759389>
- Zhu, X., Ge, Y., Li, T., Thongphiew, D., Yin, F.-F., Wu, Q.J., 2011. A planning quality evaluation tool for prostate adaptive IMRT based on machine learning. *Med. Phys.* 38, 719–726. <https://doi.org/10.1118/1.3539749>

VITA

Daniel El Basha was born in Mayaguez, Puerto Rico. In 2019, he received a Bachelor of Science in Biomedical Engineering from the University of Florida. He completed an undergraduate research thesis on computational modeling for the stereotactic treatment of age-related macular degeneration. Subsequently, he entered The University of Texas MD Anderson Cancer Center UTHHealth Houston Graduate School of Biomedical Sciences that same year. After his graduate studies, Daniel will conduct research as a research assistant before pursuing a clinical physics residency and aiming to become a board-certified medical physicist.